

## UC Davis

### UC Davis Previously Published Works

**Title**

ZmCCD8 regulates sugar and amino acid accumulation in maize kernels via strigolactone signalling.

**Permalink**

<https://escholarship.org/uc/item/1358g8v7>

**Journal**

Plant Biotechnology Journal, 23(2)

**Authors**

Zhong, Yanting

Wang, Yongqi

Pan, Xiaoying

et al.

**Publication Date**






2025-02-01

**DOI**

10.1111/pbi.14513

Peer reviewed

# ZmCCD8 regulates sugar and amino acid accumulation in maize kernels via strigolactone signalling

Yanting Zhong<sup>1,2</sup>, Yongqi Wang<sup>1</sup>, Xiaoying Pan<sup>1</sup>, Ruifeng Wang<sup>1</sup>, Dongdong Li<sup>3</sup>, Wei Ren<sup>4</sup> , Ziyi Hao<sup>5</sup>, Xiongao Shi<sup>1</sup>, Jingyu Guo<sup>2</sup>, Elia Ramarojaona<sup>6</sup>, Mario Schilder<sup>6</sup>, Harro Bouwmeester<sup>6</sup>, Limei Chen<sup>7</sup> , Peng Yu<sup>8</sup>, Jijun Yan<sup>9</sup>, Jinfang Chu<sup>9,10</sup>, Yanjun Xu<sup>11</sup>, Wenxin Liu<sup>3</sup>, Zhaobin Dong<sup>3</sup>, Yi Wang<sup>7</sup> , Xiaolan Zhang<sup>2</sup> , Fusuo Zhang<sup>1</sup> and Xuexian Li<sup>1,\*</sup> 

<sup>1</sup>State Key Laboratory of Nutrient Use and Management, College of Resources and Environmental Sciences, China Agricultural University, Beijing, China

<sup>2</sup>Beijing Key Laboratory of Growth and Developmental Regulation for Protected Vegetable Crops, Department of Vegetable Sciences, China Agricultural University, Beijing, China

<sup>3</sup>College of Agronomy and Biotechnology, China Agricultural University, Beijing, China

<sup>4</sup>College of Grassland Science and Technology, China Agricultural University, Beijing, China

<sup>5</sup>Department of Ecology and Ecological Engineering, China Agricultural University, Beijing, China

<sup>6</sup>Plant Hormone Biology Group, Swammerdam Institute for Life Sciences, University of Amsterdam, Amsterdam, The Netherlands

<sup>7</sup>State Key Laboratory of Plant Environmental Resilience, Center for crop functional genomics and molecular breeding, College of Biological Science, China Agricultural University, Beijing, China

<sup>8</sup>Emmy Noether Group Root Functional Biology, Institute of Crop Science and Resource Conservation, University of Bonn, Bonn, Germany

<sup>9</sup>National Centre for Plant Gene Research (Beijing), Institute of Genetics and Developmental Biology, Chinese Academy of Sciences, Beijing, China

<sup>10</sup>University of Chinese Academy of Sciences, Beijing, China

<sup>11</sup>Department of Applied Chemistry, China Agricultural University, Beijing, China

Received 26 February 2024;

revised 6 September 2024;

accepted 23 October 2024.

\*Correspondence (Tel +86 10 6273 3640;

fax +86 10 6273 1016; email [steve@cau.edu.cn](mailto:steve@cau.edu.cn))

[steve@cau.edu.cn](mailto:steve@cau.edu.cn))

## Summary

How carbon (sucrose) and nitrogen (amino acid) accumulation is coordinatively controlled in cereal grains remains largely enigmatic. We found that overexpression of the strigolactone (SL) biosynthesis gene *CAROTENOID CLEAVAGE DIOXYGENASE 8* (*CCD8*) resulted in greater ear diameter and enhanced sucrose and amino acid accumulation in maize kernels. Loss of *ZmCCD8* function reduced kernel growth with lower sugar and amino acid concentrations. Transcriptomic analysis showed down-regulation of the transcription factors *ZmMYB42* and *ZmMYB63* in *ZmCCD8* overexpression alleles and up-regulation in *zmccd8* null alleles. Importantly, *ZmMYB42* and *ZmMYB63* were negatively regulated by the SL signalling component UNBRANCHED 3, and repressed expression of the sucrose transporters *ZmSWEET10* and *ZmSWEET13c* and the lysine/histidine transporter *ZmLHT14*. Consequently, null alleles of *ZmMYB42* or *ZmMYB63* promoted accumulation of soluble sugars and free amino acids in maize kernels, whereas *ZmLHT14* overexpression enhanced amino acid accumulation in kernels. Moreover, overexpression of the SL receptor *DWARF 14B* resulted in more sucrose and amino acid accumulation in kernels, down-regulation of *ZmMYB42* and *ZmMYB63* expression, and up-regulation of *ZmSWEETs* and *ZmLHT14* transcription. Together, we uncover a distinct SL signalling pathway that regulates sucrose and amino acid accumulation in kernels. Significant association of two SNPs in the 5' upstream region of *ZmCCD8* with ear and cob diameter implicates its potential in breeding toward higher yield and nitrogen efficiency.

**Keywords:** CCD8, strigolactone, maize, sugar transporter, amino acid transporter.

## Introduction

Carbon and nitrogen allocation are among the most important and extremely sophisticated biological processes to determine crop yield (Bihmidine *et al.*, 2013; Guo *et al.*, 2020a; Lalonde *et al.*, 2004; Yang *et al.*, 2022). Until now, only several co-regulators of carbon/nitrogen transport have been characterized. ELONGATED HYPOCOTYL 5 (HY5) regulates *SUGARS WILL EVENTUALLY BE EXPORTED TRANSPORTER 11* and 12 (*SWEET11* and 12) for sugar efflux in the leaf and induces *NITRATE TRANSPORTER 2.1* (*NRT2.1*) expression for nitrate uptake in *Arabidopsis* roots (Chen *et al.*, 2016). In rice, GROWTH-REGULATING FACTOR 4 (GRF4) promotes expression of the sugar transporter *SWEET11* in the shoot and of nitrogen

transporters in the root (Li *et al.*, 2018). SUCROSE and GLUCOSE CARRIER 1 (*ZmSUGCAR1*) directly transports sugars and nitrate from the basal endosperm transfer layer during kernel growth; loss of *ZmSUGCAR1* function hinders grain filling and leads to smaller kernels in maize (*Zea mays* L.) (Yang *et al.*, 2022).

How to co-regulate transport of sugars and amino acids to maximize crop production under constantly changing conditions remains a fundamental biological question to be investigated. Maize is a worldwide, staple food and feed crop, whose grain yield is dependent upon proper ear development and robust kernel growth after silking (Cantarero *et al.*, 1999; Hawkins and Cooper, 1981). Kernel development is established during a critical period, 2-to-3 weeks after pollination (Schussler and

Westgate, 1991; Tollenaar *et al.*, 1992). Sugars and nitrogen assimilates are co-ordinately allocated for kernel setting and grain filling via the central cob (Crawford *et al.*, 1982; Pan *et al.*, 2015). Sugar translocation is partly mediated by SWEETs and sucrose transporters (SUCs) (Bihmidine *et al.*, 2013; Braun *et al.*, 2014). SWEET functions as a sucrose or hexose uniporter, contributing to phloem loading and grain filling (Bezruczyk *et al.*, 2018; Sosso *et al.*, 2015; Xuan *et al.*, 2013). As to nitrogen assimilates, lysine/histidine transporters (LHTs) are high-affinity broad-spectrum amino acid transporters important for plant growth and biomass accumulation (Chen and Bush, 1997; Guo *et al.*, 2020a; Hirner *et al.*, 2006; Schobert and Komor, 1990; Tegeder and Rentsch, 2010; Wang *et al.*, 2021).

Strigolactones (SLs) are a class of carotenoid-derived phytohormones primarily synthesized in the root. Secretion of SL into the soil stimulates branching of arbuscular mycorrhizal fungi that symbiotically enhance the host plant's nutrient acquisition. Acropetal SL transport to the shoot regulates branching, and organ development and growth (Akiyama *et al.*, 2005; Czarnecki *et al.*, 2013; Gomez-Roldan *et al.*, 2008; Ha *et al.*, 2014; Kapulnik and Koltai, 2014; Sasse *et al.*, 2015; Sun *et al.*, 2023; Ueda and Kusaba, 2015; Umehara *et al.*, 2008). Bioactive SLs are synthesized from  $\beta$ -carotene cleavage mediated by a series of conserved enzymes in the angiosperms (Alder *et al.*, 2012; Lin *et al.*, 2009). CAROTENOID CLEAVAGE DIOXYGENASE 7 (CCD7; MORE AXILLARY GROWTH 3/MAX3) cleaves the 9',10' double bond of 9-*cis*- $\beta$ -carotene to generate 10'-apo- $\beta$ -carotenal, and the latter is converted by CCD8 to produce carlactone as a SL intermediate *in vivo* (Alder *et al.*, 2012; Arite *et al.*, 2007; Snowden *et al.*, 2005; Zou *et al.*, 2006). Different *ccd8* mutant plants display species-dependent phenotypes in shoot branching, and root, fruit, and ear growth (Arite *et al.*, 2007; Auldridge *et al.*, 2006; Guan *et al.*, 2012; Kohlen *et al.*, 2012). A recent study shows that *ZmCCD8* contributes to reducing the thickness of the cupulate fruitcase (seed coat) of maize kernels; *TEOSINTE GLUME ARCHITECTURE 1* (*TGA1*) is another regulator of seed coat that was prominently selected during maize domestication (Guan *et al.*, 2022). Carlactone is oxidized either by the cross-species cytochrome P450 monooxygenase MAX1 (Abe *et al.*, 2014; Yoneyama *et al.*, 2018; Zhang *et al.*, 2014) or the newly discovered *ZmCYP706C37* (Li *et al.*, 2023) in maize. In combination with carlactonoic acid methyltransferase, *ZmCLAMT1*, this results in the formation of different active SLs, including zealactone, zeapyranolactone, zealactol, zealactonoic acid and 3-oxo-methyl- carlactonoic acid (Li *et al.*, 2023). The strigolactone receptor  $\alpha/\beta$ -hydrolase DWARF 14 (D14) perceives SL, and subsequently interacts with an F-box and leucine-rich repeat protein DWARF 3 (D3; MAX2) to trigger ubiquitination and degradation of the critical repressor DWARF 53 (D53; SMXL6/7/8) (Jiang *et al.*, 2013; Wang *et al.*, 2020; Zhou *et al.*, 2013). D53 interacts with UNBRANCHED 3 (UB3) and TASSEL SHEATH 4 (TSH4) to regulate male and female inflorescence development in maize (Liu *et al.*, 2021). In rice, D53 also suppresses functions of the UB3 homologue IPA1 (Jiang *et al.*, 2013; Song *et al.*, 2017). Only a limited number of downstream transcription modulators of SL signalling have been reported, i.e., BRANCHED 1 (BRC1), TCP DOMAIN PROTEIN 1 (TCP1) and PRODUCTION OF ANTHOCYANIN PIGMENT 1 (PAP1, a MYB transcription factor), which control shoot branching, leaf elongation and anthocyanin accumulation, respectively (Wang *et al.*, 2020). MYB transcription factors *TaODORANT1* and *ZmMYB14* are also involved in carbon

and nitrogen storage in cereal grains (Luo *et al.*, 2021; Xiao *et al.*, 2017).

Notably, biological functions of *ZmCCD8* in regulating ear growth and underlying mechanisms along SL signalling are still largely unknown. Here, we found that *ZmCCD8* overexpression results in greater ear and cob diameter with more abundant soluble sugars and free amino acids in the kernel. The transcription factors *ZmMYB42* and *ZmMYB63* bind and repress expression of the sucrose transporters *ZmSWEET10* and *ZmSWEET13c* and the amino acid transporter *ZmLHT14*, to modulate accumulation of soluble sugars and free amino acids. Together with *ZmD14B* and *ZmLHT14* overexpression lines and biochemical and GWAS analysis, we reveal a previously uncharacterized SL signalling module that mediates sugar and amino acid transport in maize, with great potential for high-yield breeding.

## Results

### *ZmCCD8* promoted accumulation of soluble sugars and free amino acids in the maize kernel

*ZmCCD8* is highly expressed in the root and ear during flowering time (Guan *et al.*, 2012). Notably, *ZmCCD8* transcription levels gradually declined in the ear from the silking stage to 3 weeks after pollination (Figure S1). We employed two independent CRISPR/Cas9 edited lines (*zmccd8-1* & *zmccd8-2*) and two representative overexpression lines (*ZmCCD8-OE1* & *ZmCCD8-OE2*) of *ZmCCD8* (Figure 1a,b) to investigate how *ZmCCD8* regulates ear and kernel growth (Figure 1c). Zealactone, a major SL in maize, was not detected in the root of *zmccd8* lines, but significantly over-accumulated in *ZmCCD8* overexpression lines as compared to wild-type (WT; Figure 1d). *ZmCCD8* knockout and overexpression generated opposing effects on shoot and ear growth (Figure 1c; Figure S2a). In detail, two *zmccd8* lines bore shorter, thinner and lighter ears at maturity when compared with the WT (Figure 1c,e-h; Figure S2b-f), as well as lower kernel weight per ear and 100-kernel weight (Figure 1i,j). In contrast, *ZmCCD8* overexpression plants had longer, thicker and heavier ears than WT plants (Figure 1c,e-h; Figure S2b-f). Kernel weight per ear of *ZmCCD8* overexpression lines was greater than in WT siblings, although 100-kernel weight remained unchanged in *ZmCCD8* overexpression lines (Figure 1i, j). In contrast, kernel row number did not change between transgenic and WT plants (Figure 1k; Figure S2g). Agronomically, significant decreases in 100-kernel weight of *zmccd8* lines (Figure 1j) may trace back to insufficient carbon (soluble sugars) and nitrogen (free amino acids) flow during grain filling. Then, we analysed sugar and amino acid concentrations in kernels at 7 and 21 days after pollination (7 DAP & 21 DAP). In the field, soluble sugar concentrations were at similar levels in transgenic and WT kernels at 7 DAP (Figure 1l), whereas concentrations were significantly decreased by 12.35% and 8.10% in two knockout lines and increased by 18.60% and 13.10% in two overexpression lines at 21 DAP, as compared with WT plants (Figure 1l). In particular, sucrose concentration was 26.64% and 19.47% lower in kernels of two *zmccd8* lines at 21 DAP, and 36.48 and 37.70% higher in *ZmCCD8* overexpression kernels (Figure 1m) as respectively compared to WT. Glucose and fructose concentrations were unchanged in transgenic versus WT kernels (Figure 1m). Similarly, the two *zmccd8* lines had 16.45% and 11.53% lower free amino acid concentrations, and two overexpression lines displayed

35.23% and 25.67% higher concentrations of free amino acids at 21 DAP, compared to the WT (Figure 1n). Moreover, concentrations of alanine,  $\beta$ -alanine, aspartic acid, glycine and serine were significantly decreased in *zmccd8* mutant lines, whereas alanine and arginine levels were increased in *ZmCCD8* overexpression kernels (Table 1).

### Transcriptome analysis of the kernel of *ZmCCD8* transgenic plants

To identify the genes that regulate the accumulation of soluble sugars and free amino acids in maize kernels, we performed transcriptome profiling at 7 DAP and found 401 differentially expressed genes (DEGs) in *zmccd8* kernels and 3593 DEGs in kernels overexpressing *ZmCCD8* as compared to WT (Figure 2a; Tables S1 and S2). Pathway enrichment analyses showed that these DEGs were correlated with cell cycle organization, solute transport, as well as carbohydrate metabolism and amino acid metabolism (Figure 2a,b). Importantly, 106 DEGs had opposite expression patterns in *zmccd8* and *ZmCCD8-OE* lines, with 48 annotated genes (Figure 2a,c). Of particular interest, expression of the sugar transporter genes *SWEET10* and *SWEET13c* and of the amino acid transporter gene *LHT14* were significantly down-regulated in *zmccd8* lines, but up-regulated in the *ZmCCD8* overexpression lines. Transcript accumulation of the transcription factor genes *ZmMYB42* and *ZmMYB63* was enhanced in *zmccd8* knockouts and reduced after *ZmCCD8* overexpression (Figure 2c; Figure S3a–e). Taken together, these data suggest that *ZmMYB42* and *ZmMYB63* expression are regulated by *ZmCCD8* and SL signalling.

### *ZmMYB42* and *ZmMYB63* directly repressed the expression of transporters *ZmSWEET10*, *ZmSWEET13c* and *ZmLHT14*

We next examined subcellular localization of the three candidate transporters. GFP-tagged *ZmSWEET10*, *ZmSWEET13c* and *ZmLHT14* localized to the plasma membrane in leaf cells of *Nicotiana benthamiana* (Figure S4a). When expressed in a sucrose uptake defective yeast strain (SUSY7/ura3), both *ZmSWEET10* and *ZmSWEET13c* were able to enhance sucrose absorption as *Arabidopsis* sucrose transporter 2 (SUC2) does (Figure 2d) (Srivastava et al., 2008).

MYB transcription factors affect sugar accumulation in strawberry and are involved in storage protein biosynthesis in wheat (Luo et al., 2021; Wei et al., 2018). Promoter analysis revealed *cis*-elements correlated with MYB protein binding (MBS: TAACTG or CCGTTG) in the promoter regions of *ZmSWEET10*, *ZmSWEET13c* and *ZmLHT14* (Figure 3a). Thus, we considered whether *ZmMYB42* and *ZmMYB63* directly regulate expression of *ZmSWEETs* and *ZmLHT14*, contributing to accumulation

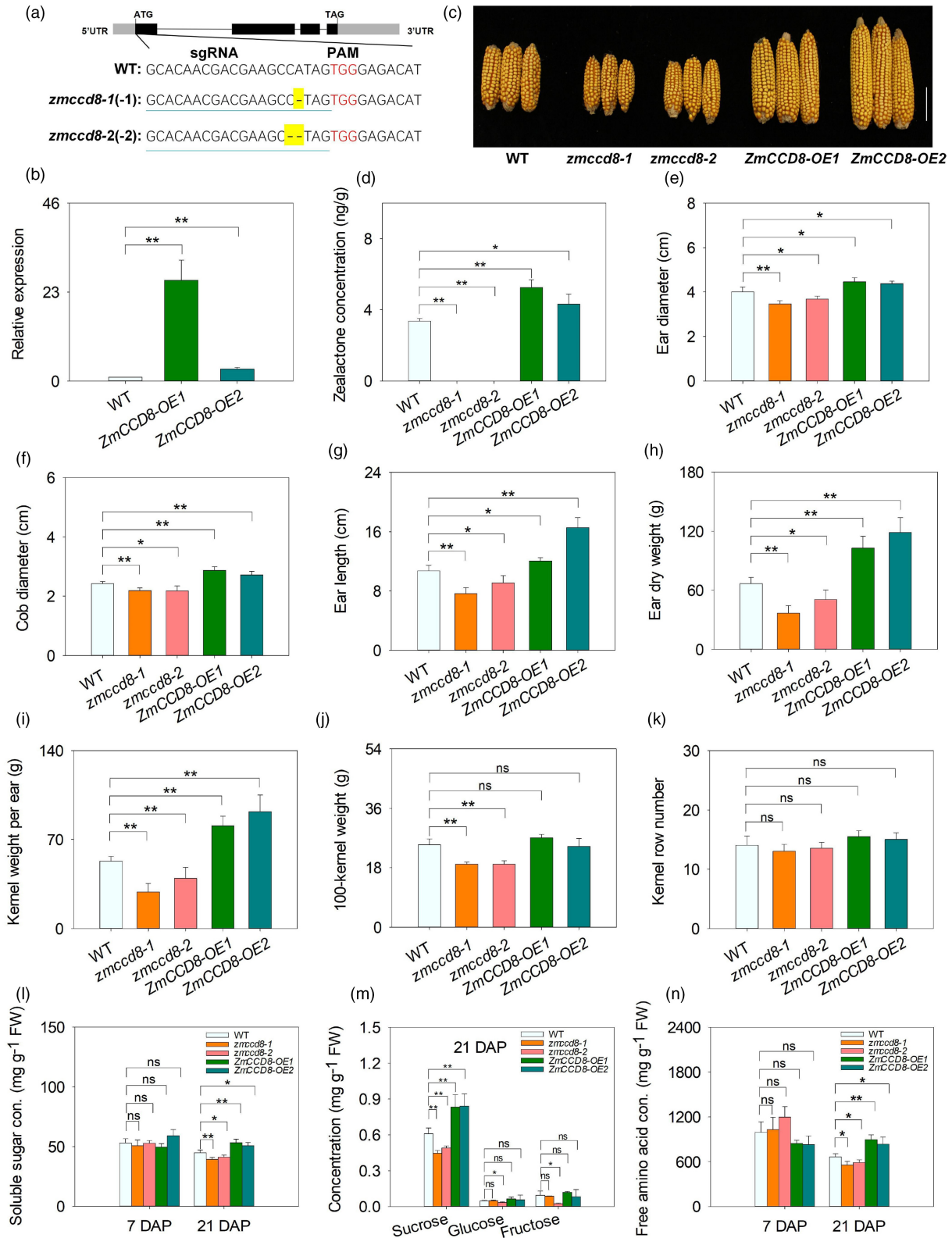
of soluble sugars and free amino acids in kernels. Transient expression in *Nicotiana benthamiana* localized *ZmMYB42* and *ZmMYB63* proteins to the nucleus (Figure S4b). Yeast one-hybrid (Y1H) assays suggested binding of *ZmMYB42* and *ZmMYB63* to the promoter region of *ZmSWEET10*, *ZmSWEET13c* and *ZmLHT14* (Figure 3b). The electrophoresis mobility shift assay (EMSA) and corresponding retardation in mobility verified biochemical interaction of *ZmMYB42* and *ZmMYB63* with the MBS oligonucleotides of three transporters *in vitro* (Figure 3c,d). Further verification of these interactions *in vivo*, chromatin immunoprecipitation–quantitative PCR (ChIP-qPCR), was carried out using maize protoplasts. Significant enrichment of MBS-containing sequences in immunoprecipitated fractions suggested direct binding of *ZmMYB42* and *ZmMYB63* to the promoter of *ZmSWEET10*, *ZmSWEET13c* and *ZmLHT14* (Figure 3e–j). Lastly, a dual-luciferase reporter (DLR) assay in *Nicotiana benthamiana* leaves indicated that *ZmMYB42* and *ZmMYB63* may repress expression of two *ZmSWEET* transporters and the amino acid transporter *ZmLHT14* *in planta* (Figure 3k,l).

### Knockout of *ZmMYB42* and *ZmMYB63* promoted accumulation of soluble sugars and free amino acids in kernels

CRISPR/Cas9 edited loss of function alleles of *ZmMYB42* (*zmmyb42-1* & *zmmyb42-2*) and *ZmMYB63* (*zmmyb63-1* & *zmmyb63-2*) were generated (Figure 4a,b). Expression of *ZmSWEET10*, *ZmSWEET13c* and *ZmLHT14* were up-regulated in *zmmyb42* and *zmmyb63* kernels at 7 DAP (Figure 4c,d). Importantly, the soluble sugar concentration of both *zmmyb42* and *zmmyb63* kernels significantly increased at 7 and 21 DAP, as compared to WT (Figure 4e,f). In particular, the concentration of sucrose was 50.00% and 38.39% higher in *zmmyb42* kernels, and 19.04% and 33.39% higher in *zmmyb63* kernels at 21 DAP, respectively (Figure 4g,h). Free amino acid concentrations of *zmmyb42* and *zmmyb63* kernels were unaffected at 7 DAP as compared to WT kernels (Figure 4i,j); however, the amino acid levels were 31.78% and 20.85% higher in *zmmyb42* kernels at 21 DAP, respectively, as compared to the WT kernels (Figure 4i), including more alanine,  $\beta$ -alanine, arginine, glutamine, isoleucine, lysine, methionine, threonine and valine (Table 1) in both *zmmyb42-1* and *zmmyb42-2* lines. Similarly, free amino acids were 31.05% and 22.95% more abundant in *zmmyb63* kernels at 21 DAP, respectively, when compared with the WT kernels (Figure 4j), with higher concentrations of alanine,  $\beta$ -alanine, threonine and valine in *zmmyb63-1* and *zmmyb63-2* lines (Table 1). Thus, *ZmMYB42* and *ZmMYB63* regulate the accumulation of soluble sugars and free amino acids in kernels via transcriptional repression of *ZmSWEETs* and *ZmLHT14*.

**Figure 1** The ear phenotype of stable transgenic lines of *ZmCCD8* at the reproductive stage. (a) Gene structure of *ZmCCD8* and mutation sites of representative *zmccd8* mutant lines. The black boxes represent exons, the lines represent introns and the grey boxes represent the untranslated regions. The sgRNA target sequence is underlined and the PAM motif is highlighted in red. The single bp (A) deletion in the knockout line 1 (*zmccd8-1*) and two bp (CA) deletion in the knockout line 2 (*zmccd8-2*) are highlighted. (b) Relative expression of *ZmCCD8* in kernels of two representative overexpression lines at 7 days after pollination (DAP). (c) Ears at maturity of two *ZmCCD8* knockout (*zmccd8-1*, *zmccd8-2*) and overexpression (*ZmCCD8-OE1*, *ZmCCD8-OE2*) lines. (d) SL levels in the root of *ZmCCD8* knockout and overexpression lines. (e–j) Ear diameter (e) and cob diameter (f), ear length (g), ear dry weight (h), kernel weight per ear (i), 100-kernel weight (j), and kernel row number (k) of *ZmCCD8* knockout and overexpression lines. (l–n) Soluble sugar (l), individual sugar (m), and free amino acid (n) concentrations (con.) in kernels of *ZmCCD8* knockout and overexpression lines at 7 days (7 DAP) or 21 days (21 DAP) after pollination. Error bars represent the SD of three (b) or four (d–n) biological replicates. Asterisks indicate significant differences relative to WT as determined by the two-tailed Student's *t*-test (\**P* < 0.05; \*\**P* < 0.01). The scale bar = 5 cm. ns, no significant difference.





**ZmLHT14 promoted amino acid accumulation in kernels**

To evaluate *ZmLHT14*'s contribution to amino acid accumulation in kernels at 21 DAP, we generated *ZmLHT14* overexpression plants and selected two representative lines (46.9- and 38.8-fold

higher expression, respectively) for further study (Figure 5a). The free amino acid concentrations increased by 20.31% and 10.47% in kernels from two *ZmLHT14* overexpression lines at 21 DAP (Figure 5b) due to enhanced accumulation of alanine,  $\beta$ -alanine, isoleucine, lysine, methionine and threonine (Table 1).

**Table 1** Concentrations of individual amino acids in kernels of *ZmCCD8*, *ZmMYB42*, *ZmMYB63*, *ZmLHT14* and *ZmD14B* transgenic lines and corresponding WT plants at 21 DAP

Genotype	$\beta$ -Ala	Ala	Arg	Asp	Asn	Glu	Gln	Gly	Orn
WT	4.77 ± 0.72	125.62 ± 11.90	3.59 ± 0.20	56.41 ± 5.03	6.74 ± 0.39	64.74 ± 3.19	68.43 ± 19.16	36.20 ± 5.75	0.41 ± 0.13
<i>zmccd8-1</i>	3.20 ± 0.86*	103.59 ± 8.79*	4.15 ± 0.44	44.20 ± 7.78*	5.47 ± 1.60	51.03 ± 8.63*	69.83 ± 5.24	24.29 ± 3.48*	0.23 ± 0.02*
<i>zmccd8-2</i>	3.02 ± 0.36**	99.22 ± 15.55*	3.91 ± 0.23	41.89 ± 3.11**	5.46 ± 0.43*	62.97 ± 10.07	66.86 ± 7.45	23.80 ± 4.16*	0.22 ± 0.02*
<i>ZmCCD8-OE1</i>	3.88 ± 0.27	153.36 ± 6.84**	4.81 ± 0.58**	51.95 ± 4.74	5.84 ± 0.91	67.57 ± 10.25	91.69 ± 14.88	33.69 ± 4.43	0.32 ± 0.02
<i>ZmCCD8-OE2</i>	4.11 ± 0.75	146.05 ± 9.03*	4.80 ± 0.38**	48.33 ± 5.01	7.10 ± 1.55	69.41 ± 7.55	87.48 ± 9.11	32.04 ± 2.14	0.30 ± 0.03
WT	1.79 ± 0.32	53.20 ± 3.81	4.08 ± 0.16	40.39 ± 5.70	10.61 ± 3.53	62.63 ± 4.94	26.70 ± 2.11	8.24 ± 0.27	0.16 ± 0.03
<i>zmmyb42-1</i>	3.25 ± 0.58*	76.28 ± 17.88*	7.02 ± 2.17*	48.99 ± 4.45	18.52 ± 7.89	71.47 ± 12.84	77.32 ± 26.71**	10.52 ± 2.19	0.33 ± 0.14
<i>zmmyb42-2</i>	3.19 ± 0.45**	82.74 ± 11.61**	7.17 ± 1.49**	48.93 ± 3.47*	23.16 ± 7.74*	70.07 ± 2.96*	87.94 ± 22.82**	10.21 ± 2.09	0.39 ± 0.32
WT	1.50 ± 0.32	56.41 ± 5.16	4.49 ± 0.73	41.01 ± 8.20	12.22 ± 7.03	56.74 ± 4.05	24.66 ± 3.97	8.00 ± 0.68	0.17 ± 0.11
<i>zmmyb63-1</i>	2.69 ± 0.14**	70.34 ± 9.10*	4.91 ± 0.21	44.55 ± 5.23	21.35 ± 11.08	61.39 ± 6.70	62.17 ± 8.29**	8.01 ± 0.49	0.11 ± 0.04
<i>zmmyb63-2</i>	2.01 ± 0.24*	127.07 ± 38.14*	7.99 ± 3.30	44.92 ± 5.73	10.05 ± 2.88	79.43 ± 10.50*	49.74 ± 21.16	14.73 ± 3.82*	0.18 ± 0.05
WT	2.44 ± 0.66	71.61 ± 14.28	6.17 ± 0.83	55.11 ± 10.75	59.00 ± 10.13	163.86 ± 18.06	77.39 ± 16.21	8.46 ± 2.92	0.36 ± 0.05
<i>ZmLHT14-OE1</i>	3.48 ± 0.42*	107.47 ± 18.39*	6.36 ± 0.84	64.89 ± 9.17	77.09 ± 13.06	302.80 ± 122.05	100.75 ± 14.71	12.66 ± 2.99	0.43 ± 0.04
<i>ZmLHT14-OE2</i>	4.70 ± 0.52**	93.89 ± 7.69*	7.24 ± 0.76	55.88 ± 2.27	58.46 ± 8.00	201.58 ± 25.18	86.11 ± 8.64	10.71 ± 2.60	0.40 ± 0.04
WT	2.73 ± 0.22	76.47 ± 12.78	7.23 ± 0.80	60.84 ± 4.03	66.48 ± 5.83	209.14 ± 15.36	82.81 ± 8.91	10.84 ± 2.03	0.43 ± 0.05
<i>ZmD14B-OE1</i>	4.92 ± 0.51**	139.23 ± 16.98**	8.64 ± 1.84	66.01 ± 3.38	69.77 ± 21.34	245.90 ± 46.88	104.12 ± 10.95*	18.25 ± 4.30*	0.64 ± 0.24
<i>ZmD14B-OE2</i>	3.73 ± 0.57*	127.43 ± 28.95*	8.88 ± 2.22	62.68 ± 4.31	52.95 ± 25.20	230.08 ± 47.02	121.45 ± 30.30	20.62 ± 6.46*	0.37 ± 0.09

Note: Asterisks indicate significant differences relative to WT as determined by the two-tailed Student's *t*-test (\* $P < 0.05$ ; \*\* $P < 0.01$ ). Unit, mg g<sup>-1</sup> DW.

These data indicate that *ZmLHT14* efficiently promotes amino acid accumulation in maize kernels. Notably, the soluble sugar concentration was unchanged by *ZmLHT14* overexpression (Figure 5c,d).

### UB3 bound directly to the GTAC elements of *ZmMYB42* and *ZmMYB63*

The D53-UB3 module is a well-known SL signalling component; *d53* (gain-of-function) alleles condition smaller ears (Liu et al., 2021). *ZmUB3* expression was up-regulated in *ZmCCD8* overexpression kernels, although *ZmD53* transcript accumulation was unchanged (Figure S3f,g). Interestingly, *ZmMYB42* and *ZmMYB63* harboured GTAC motifs (the core UB3 binding site) in their promoter region (Figure 6a). Y1H assay suggested that UB3 did bind to the GTAC motif of *ZmMYB42* and *ZmMYB63*, and mutation of the GTAC motif abolished such binding (Figure 6b). Our EMSA assay verified *in vitro* binding of UB3 to the GTAC motifs of both *ZmMYB42* and *ZmMYB63* (Figure 6c). ChIP-qPCR assay using transgenic maize protoplasts confirmed the significant enrichment of the F7 or F9 fragment (GTAC motif containing sequence) and affirmed the *in vivo* interaction of UB3 with target transcription factors *ZmMYB42* and *ZmMYB63* (Figure 6d,e). The DLR assay suggested that UB3 repressed *ZmMYB42* and *ZmMYB63* transcription *in planta* (Figure 6f).

### *ZmD14B*-mediated sugar and amino acid accumulation

*CCD8* functions as a plant SL biosynthesis enzyme (Arite et al., 2007; Auldrige et al., 2006; Czarniecki et al., 2013). To test whether SL is involved in the regulation of sugar and amino acid accumulation in maize kernels, we generated *ZmD14B* (the SL receptor) overexpression lines, two of whom (12.3- and 8.6-fold higher *ZmD14B* expression, respectively) were selected for further analysis (Figure 7a). *ZmD14B* overexpression resulted in higher soluble sugar concentrations at 21 DAP in two lines, and particularly enhanced sucrose accumulation by 42.12% and 36.27%, respectively (Figure 7b,c). Concentrations of free amino acids in kernels also increased by 23.41% and 16.79%, respectively, including more abundant alanine,  $\beta$ -alanine, glycine, isoleucine, leucine, lysine, methionine, serine, threonine, tryptophan, tyrosine and valine (Figure 7d; Table 1). Importantly, *ZmMYB42* and *ZmMYB63* expression was down-regulated, and

*ZmSWEET10*, *ZmSWEET13c* and *ZmLHT14* expression was up-regulated in *ZmD14B* overexpression kernels, in agreement with expression patterns of these five genes in the *ZmCCD8* overexpression kernels (Figures 2c and 7e).

### Natural variations of *ZmCCD8* were associated with ear growth in maize

Carbon and nitrogen accumulation lay the foundation for ear growth (Hirel et al., 2007; Martin et al., 2006; Sosso et al., 2015), and the cob serves as a central assimilate transfer conduit supporting ear growth, kernel establishment and grain filling. Thinner ears and cobs of *zmccd8* plants and thicker ears and cobs of *ZmCCD8* overexpression lines (Figure 1c,e,f; Figure S2b–e) demonstrate that *ZmCCD8* modulates ear and cob diameter. To identify the potential genetic correlation between natural variations of *ZmCCD8* and the ear phenotype, we carried out a GWAS survey based on a public database (Liu et al., 2017; Yang et al., 2014) and found several single-nucleotide polymorphic (SNP) loci associated with maize cob diameter (Figure 8a; Table S3). Individual SNPs conferred 3.03% to 6.43% of phenotypic variance. Of particular interest was a SNP (chr3.S\_197020433, 1204 bp upstream of the start codon) in *ZmCCD8* that is significantly associated with cob diameter ( $P = 4.82 \times 10^{-5}$ ; Figure 8a). This SNP is located in one of presumed core binding sites of MYB transcription factors for transcriptional modulation (Figure S5a,b). Higher expression levels of the 'C' haplotype were positively correlated with thicker cobs of corresponding inbred lines compared with the 'A' haplotype (Figure 8b–d). Moreover, a neighbouring genetically linked SNP (chr3.S\_197020327, 1098 bp upstream of the start codon of *ZmCCD8*) was also associated with cob ( $P = 5.58 \times 10^{-5}$ ) and ear ( $P = 1.26 \times 10^{-5}$ ) diameter (Figure 8a; Figure S6a–c).

## Discussion

Coordinated carbon (sugar) and nitrogen (amino acid) transport in the maize ear is critical for ear growth and grain filling (Yang et al., 2022). Here we show, using knockout and overexpressing lines, that *ZmCCD8* positively regulates the length, diameter and kernel weight of the maize ear (Figure 1e–i). Of particular interest is our observation that grain weight is correlated with alterations

Ile	Leu	Lys	Met	Phe	Pro	Ser	Thr	Trp	Tyr	Val
7.32 ± 1.09	6.76 ± 1.45	12.64 ± 2.11	6.78 ± 1.45	3.15 ± 0.42	35.37 ± 9.78	60.93 ± 8.41	19.11 ± 6.35	0.93 ± 0.13	9.47 ± 2.12	26.46 ± 2.04
8.06 ± 1.84	6.31 ± 1.26	11.44 ± 2.79	6.20 ± 2.62	2.90 ± 0.22	26.08 ± 3.28	46.64 ± 4.49*	20.83 ± 4.47	1.23 ± 0.21	7.93 ± 1.58	23.74 ± 3.43
7.57 ± 0.38	5.95 ± 0.15	10.58 ± 0.69	5.65 ± 0.52	2.77 ± 0.49	25.21 ± 5.21	44.64 ± 5.57*	19.63 ± 1.00	1.10 ± 0.09	7.58 ± 1.11	22.15 ± 1.92*
8.22 ± 1.52	7.38 ± 0.65	12.34 ± 1.01	6.00 ± 1.05	3.48 ± 0.23	42.25 ± 5.05	58.76 ± 3.63	25.87 ± 1.89	1.22 ± 0.21	9.19 ± 0.58	27.29 ± 1.23
8.65 ± 1.12	7.34 ± 0.96	12.75 ± 0.87	6.81 ± 1.11	3.45 ± 0.58	44.06 ± 5.66	60.87 ± 4.94	26.03 ± 2.77	1.39 ± 0.29*	9.08 ± 1.68	27.45 ± 3.02
3.23 ± 0.23	3.21 ± 0.15	8.71 ± 0.50	2.13 ± 0.18	2.71 ± 0.30	50.05 ± 15.19	21.89 ± 2.42	10.66 ± 0.78	0.68 ± 0.04	4.52 ± 0.46	11.69 ± 0.63
4.57 ± 0.87*	5.64 ± 2.54	14.88 ± 4.34*	4.48 ± 0.85**	3.36 ± 0.77	63.66 ± 23.31	28.54 ± 6.59	15.18 ± 1.87**	0.85 ± 0.14	4.93 ± 0.76	17.84 ± 4.10*
4.74 ± 0.92*	5.46 ± 1.37*	15.53 ± 2.75**	4.37 ± 0.93**	3.17 ± 0.58	55.21 ± 19.97	28.20 ± 3.22*	16.71 ± 2.33*	0.89 ± 0.09*	5.02 ± 0.61	19.74 ± 3.21*
3.45 ± 0.32	3.58 ± 0.63	9.43 ± 2.91	2.42 ± 0.39	2.68 ± 0.28	46.00 ± 13.83	21.65 ± 3.98	10.51 ± 1.09	0.71 ± 0.08	4.53 ± 0.35	12.32 ± 0.92
3.90 ± 0.54	4.10 ± 0.38	12.45 ± 1.86	3.27 ± 0.77	2.65 ± 0.39	46.38 ± 9.24	24.42 ± 2.80	14.50 ± 1.20**	0.70 ± 0.09	4.47 ± 0.34	16.13 ± 1.94*
6.20 ± 1.68*	10.02 ± 5.19*	13.34 ± 4.30	4.49 ± 1.97	5.74 ± 1.55**	52.51 ± 8.78	36.11 ± 7.06*	18.60 ± 2.61**	1.02 ± 0.26	7.95 ± 1.63**	23.12 ± 5.89*
3.77 ± 0.44	4.88 ± 0.69	12.52 ± 2.28	5.98 ± 0.99	2.82 ± 0.25	56.48 ± 9.96	32.00 ± 6.13	14.36 ± 0.95	0.70 ± 0.09	2.71 ± 0.80	17.85 ± 3.88
7.75 ± 1.56**	6.66 ± 1.18*	16.93 ± 1.75*	10.02 ± 2.45*	3.30 ± 0.40	62.70 ± 10.10	44.93 ± 11.32	23.16 ± 5.45*	0.93 ± 0.21	4.94 ± 1.67	26.89 ± 6.44
6.45 ± 1.04**	5.79 ± 0.67	19.02 ± 2.14**	7.59 ± 0.63*	3.32 ± 0.21*	52.65 ± 5.50	36.38 ± 4.45	20.91 ± 1.81**	0.78 ± 0.13	3.30 ± 0.58	22.25 ± 1.65
4.59 ± 0.30	5.77 ± 0.54	15.74 ± 3.00	6.71 ± 0.36	3.36 ± 0.23	60.35 ± 4.69	33.82 ± 1.58	17.02 ± 2.20	0.77 ± 0.05	3.73 ± 0.20	19.20 ± 2.28
7.79 ± 1.22**	8.12 ± 0.79*	24.12 ± 4.39*	9.33 ± 0.91**	3.90 ± 0.59	57.52 ± 11.41	50.93 ± 7.92**	26.66 ± 4.36**	1.15 ± 0.13**	5.50 ± 0.80**	31.67 ± 4.68**
8.20 ± 1.07**	10.16 ± 3.22*	24.72 ± 4.62*	9.69 ± 2.24*	4.98 ± 0.81**	66.86 ± 8.85	49.24 ± 7.38**	26.59 ± 5.81*	1.16 ± 0.26*	6.10 ± 1.63*	33.54 ± 7.94*

in concentrations of soluble sugars and free amino acids in *ZmCCD8* knockout and overexpression kernels at the grain filling stage (21 days after pollination) (Figure 1l,n). Sucrose serves as a major carbon assimilate for grain filling (Bihmidine *et al.*, 2013; Shen *et al.*, 2022). Likewise, accumulations of glutamine, glutamate, aspartic acid, asparagine and alanine are vital for cob and kernel development (Seebauer *et al.*, 2004; Perchlik and Tegeder, 2018). Significantly reduced accumulation of sucrose and free amino acids contributes to lighter kernels in the *zmccd8* mutant; in contrast enhanced accumulation of these carbon and nitrogen assimilates leads to greater kernel weight per ear in *ZmCCD8* overexpression lines (Figure 1e–n). Thus, *ZmCCD8* mediates accumulation of soluble sugars and free amino acids during grain growth and filling.

Allocation of sucrose and amino acids into grains is ultimately controlled by transporters in the kernel, regardless of dynamic sink-source crosstalk. Transcriptome analysis revealed significant enrichment of the ‘solute transport’ pathway in the *ZmCCD8* overexpression kernels (Figure 2b). We observed opposite expression patterns of two sugar transporters (*ZmSWEET10* and *ZmSWEET13c*) and one amino acid transporter (*ZmLHT14*), with down-regulated expression in *zmccd8* mutant kernels and up-regulation in *ZmCCD8* overexpression kernels (Figure 2c). *ZmSWEET4c* mediates hexose transport across the basal endosperm transfer layer, and *zmsweet4c* mutants have defective kernels with *empty pericarp* due to impaired seed filling (Sosso *et al.*, 2015). A triple knock-out maize mutant, *zmsweet13a,b,c*, retains more sucrose in the leaves (Bezruczyk *et al.*, 2018). In *Arabidopsis*, *AtLHT1* and *AtLHT6* function in amino acid uptake from the soil and transport into leaf mesophyll cells (Hirner *et al.*, 2006). *OsLHT1* is also involved in amino acid uptake in relation to grain yield and quality (Guo *et al.*, 2020a, 2020b). We showed that plasma membrane-localized *ZmSWEET10* and *ZmSWEET13c* served as potent sucrose transporters in yeast (Figure 2d; Figure S4a), and *ZmLHT14* overexpression enhanced amino acid accumulation in transgenic maize kernels at the grain filling stage (Figure 5b). Owing to the physiological alterations in *ZmCCD8* transgenic lines, gene expression patterns and functional characterization of three transporters (*ZmSWEET10*, *ZmSWEET13c* and *ZmLHT14*), we conclude that *ZmCCD8* functions primarily as a co-regulator of transport and

accumulation of sucrose and amino acids in the kernel for grain filling/ear growth. Previous GWAS assays suggested that *ZmCCD8* is also associated with kernel length (Zhu *et al.*, 2018). Cob development is directly related to carbon and nitrogen transport (Crawford *et al.*, 1982; Pan *et al.*, 2015), with an innate link to grain filling and growth. Our GWAS analysis revealed that two linked SNPs in the *ZmCCD8* promoter region were significantly associated with cob and ear diameter (Figure 8a–d; Figure S6a–c), suggesting that *ZmCCD8* may be a target for breeding high-yield maize genotypes.

Whereas SL biosynthesis and signal perception are well described, the characterization of the downstream transcription modulators is only just beginning. Here, we identified *ZmMYB42* and *ZmMYB63* as downstream targets of SL signalling that regulate seed growth. Up-regulation of *ZmMYB42* and *ZmMYB63* expression in *zmccd8* kernels, its corresponding down-regulation in *ZmCCD8* overexpression kernels, taken together with their nuclear localization (Figure 2c; Figure S4b), suggest that both *ZmMYB42* and *ZmMYB63* are SL downstream signalling components. In strawberry, *MYB44.2* represses sucrose accumulation in fruits (Wei *et al.*, 2018). Our work demonstrates that *ZmMYB42* and *ZmMYB63* directly bind and repress the expression of *ZmSWEET10*, *ZmSWEET13c* and *ZmLHT14* (Figures 3a–l and 4c, d). Knockout alleles of *ZmMYB42* or *ZmMYB63* significantly increased the concentration of soluble sugars and free amino acids in kernels at the grain-filling stage (Figure 4e–j). Overexpression of *ZmLHT14* enhanced accumulation of free amino acids including alanine,  $\beta$ -alanine, isoleucine, lysine, methionine and threonine in kernels (Figure 5b; Table 1), indicating that *ZmLHT14* acts as an amino acid transporter *in vivo* favouring nitrogen accumulation in maize grains. *D53* suppresses *UB3* and *TSH4* activities to regulate male and female inflorescence development in maize (Kong *et al.*, 2023; Liu *et al.*, 2021). Our results show that *ZmUB3* expression is regulated by *ZmCCD8* (Figure S3f). Furthermore, *ZmUB3* directly binds to the GTAC box in the promoter of *ZmMYB42* and *ZmMYB63* to repress their expression, revealing a *ZmUB3*-mediated transcription regulatory pathway. Prior data show that in rice, the grain weight of the *d14* mutant is reduced, and a maize double mutant of *D14A* and *D14B* has a shorter ear (Guan *et al.*, 2022; Yamada *et al.*, 2018). In contrast, *ZmD14B* overexpression significantly increased the concentrations of

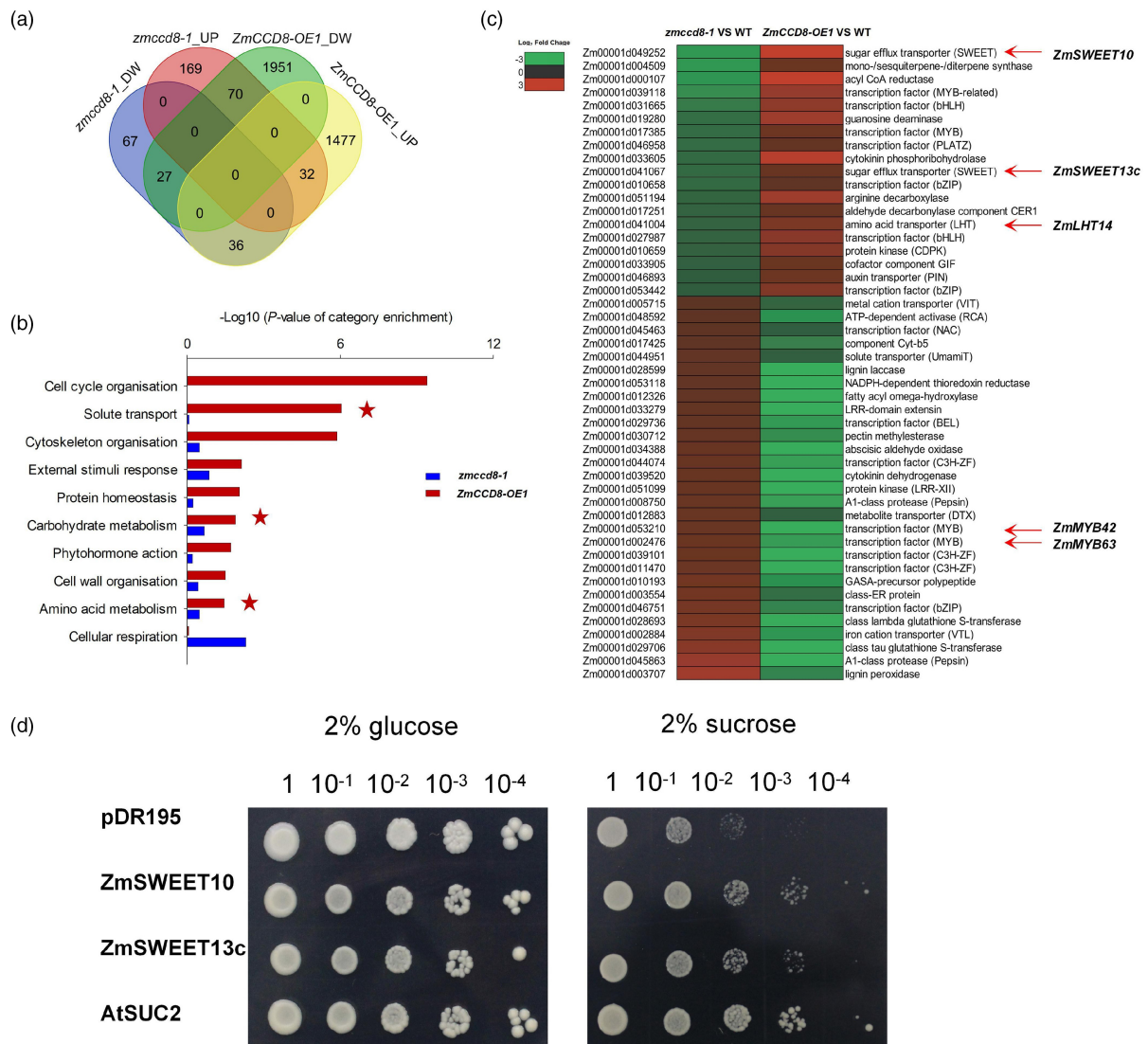


**Figure 2** The transcriptome profiling of *ZmCCD8* transgenic lines and the transport activity of *ZmSWEETs*. (a) Venn diagram of differentially expressed genes (DEGs) in the kernels of *ZmCCD8* knockout (*zmccd8-1*) and overexpression (*ZmCCD8-OE1*) lines at 7 days after pollination, as compared to WT plants. UP, up-regulated. DW, down-regulated. (b) Pathway enrichment analysis of DEGs in the kernels of *ZmCCD8* transgenic lines compared to WT plants. The stars indicate gene enrichment involved in the solute transport, carbohydrate and amino acid metabolism pathways. (c) The heat map of DEGs with opposite expression patterns in the kernels of *ZmCCD8* knockout and overexpression lines compared to WT plants. (d) Sucrose transport activities of *ZmSWEET10* and *ZmSWEET13c* in the yeast strain *SUSY7/ura3* providing 2% glucose or sucrose. The empty vector pDR195 and *AtSUC2* transformed into *SUSY7/ura3* as the negative and positive control, respectively.

sucrose and an array of free amino acids in 21 DAP kernels (Figure 7b–d). Importantly, expression of *ZmMYB42* and *ZmMYB63* was down-regulated, whereas expression of *ZmUB3*, *ZmSWEET10* and *ZmLHT14* was up-regulated in *ZmD14B* overexpression kernels, clearly affirming that SL regulates sugar and amino acid transport in maize via *ZmMYB42* and *ZmMYB63* (Figure 7e).

Taken together, we propose a model for how *ZmCCD8* regulates sugar and amino acid transport via SL signalling in maize kernels (Figure 9). In *zmccd8* mutants devoid of SL production, D53 interacts with UB3 to restrain its activity. *ZmMYB42* and *ZmMYB63* down-regulate expression of *ZmSWEET10*, *ZmSWEET13c* and *ZmLHT14*, resulting in lowered accumulation of sucrose and free amino acids in kernels and smaller ears. In *ZmCCD8* overexpression lines, enhanced *ZmCCD8* transcription promotes SL biosynthesis. SL is then perceived by

D14 to trigger D53 degradation and release the UB3 protein. UB3 subsequently represses *ZmMYB42* and *ZmMYB63* transcription, enabling up-regulation of *ZmSWEET10*, *ZmSWEET13c* and *ZmLHT14* expression, which leads to more sucrose and free amino acid accumulation supporting robust ear growth. Our work provides new avenues for molecular breeding for high-yield and nitrogen-efficient maize germplasms.

## Materials and methods

### Plant materials and growth conditions

Inbred lines B104, B73-329, *ZmCCD8* knockout and overexpression lines, *ZmMYB42* knockouts, *ZmMYB63* knockouts, *ZmD14B* and *ZmLHT14* overexpression lines were used for gene expression analysis and phenotypic observation. Negative transgenic lines of



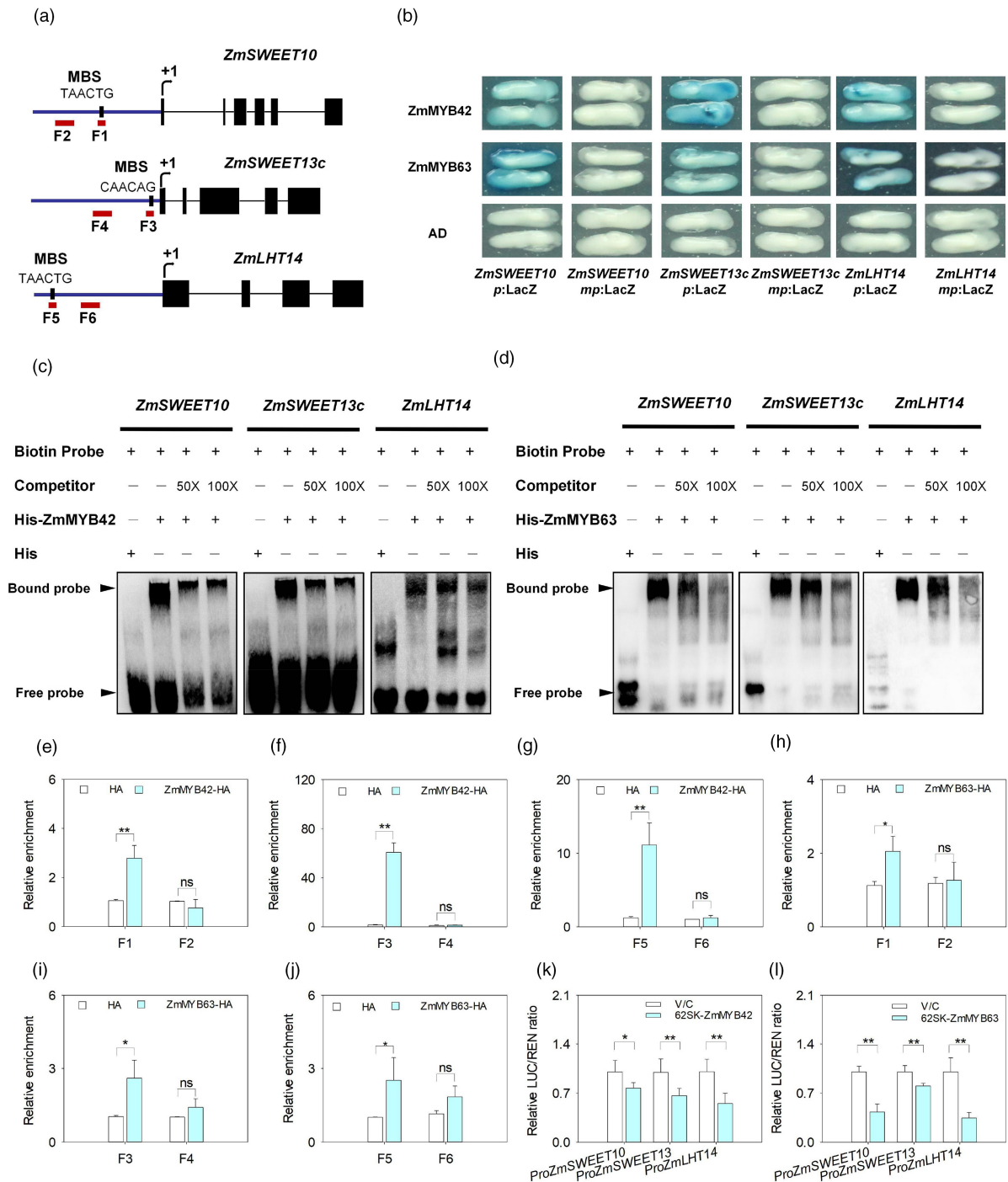


**Figure 3** Regulation of *ZmSWEETs* and *ZmLHT14* by *ZmMYBs*. (a) The MBS elements in the promoter of *ZmSWEET10*, *ZmSWEET13c* and *ZmLHT14*. Black boxes represent exons. F1/F3/F5 are MBS-containing fragments and F2/F4/F6 correspond to non-MBS control fragments. (b) Yeast one-hybrid assay showing that *ZmMYB42* and *ZmMYB63* directly bind to MBS elements of *ZmSWEET10*, *ZmSWEET13c* and *ZmLHT14*. The empty vector AD and MBS mutants (*mp*) are used as negative control. (c and d) EMSA showing binding of *ZmMYB42* and *ZmMYB63* to the biotin-labelled MBS-containing oligonucleotides of *ZmSWEET10*, *ZmSWEET13c* and *ZmLHT14* promoters. Black triangles indicate bound and free probes, respectively. (e–j) ChIP-qPCR showing binding of *ZmMYB42* (e, f, g) and *ZmMYB63* (h, i, j) to the MBS-containing elements in the promoter of *ZmSWEET10*, *ZmSWEET13c* and *ZmLHT14*. (k and l) Transient expression assay showing down-regulation of *ZmSWEET10*, *ZmSWEET13c* and *ZmLHT14* by *ZmMYB42* (62SK-*ZmMYB42*) and *ZmMYB63* (62SK-*ZmMYB63*) compared to the vector control (V/C). Error bars represent the SD of three (e–j) or five (k, l) biological replicates. Asterisks indicate significant differences relative to the vector control as determined by the two-tailed Student’s *t*-test (\**P* < 0.05; \*\**P* < 0.01).

B104 or B73-329 were used as the wild-type lines. Seedling experiments were performed in the greenhouse of China Agricultural University (Beijing) with a 14/10 h light/dark

photoperiod, 28/22 °C day/night temperature, and 60% relative humidity, following our well-established protocol (Zhong *et al.*, 2020). The nutrient solution for the hydroponic



experiments comprised of 2 mM NH<sub>4</sub>NO<sub>3</sub>, 0.25 mM KH<sub>2</sub>PO<sub>4</sub>, 0.75 mM K<sub>2</sub>SO<sub>4</sub>, 0.1 mM KCl, 2 mM CaCl<sub>2</sub>, 0.65 mM MgSO<sub>4</sub>, 0.2 mM Fe-EDTA, 1 × 10<sup>-3</sup> mM ZnSO<sub>4</sub>, 1 × 10<sup>-3</sup> mM MnSO<sub>4</sub>,

1 × 10<sup>-4</sup> mM CuSO<sub>4</sub>, 5 × 10<sup>-6</sup> mM (NH<sub>4</sub>)<sub>6</sub>Mo<sub>7</sub>O<sub>24</sub> and 1 × 10<sup>-3</sup> mM H<sub>3</sub>BO<sub>3</sub>. Each line had three biological and three technical replicates and nutrient solutions were changed every

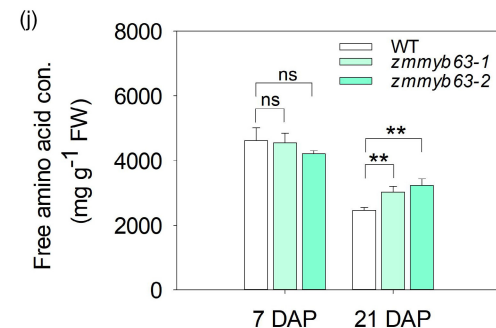
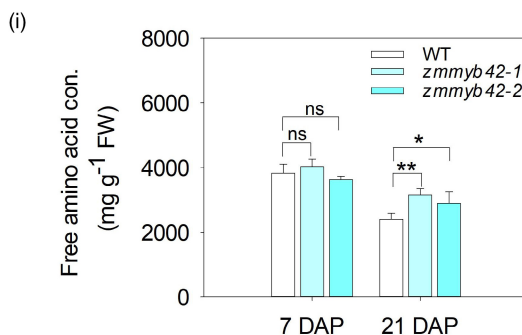
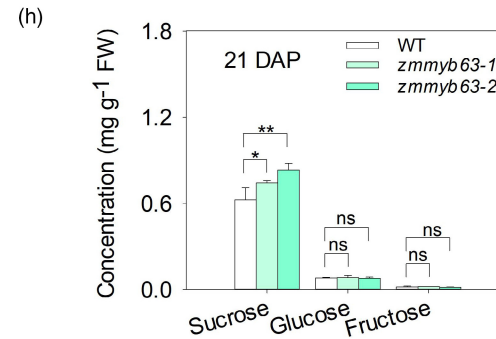
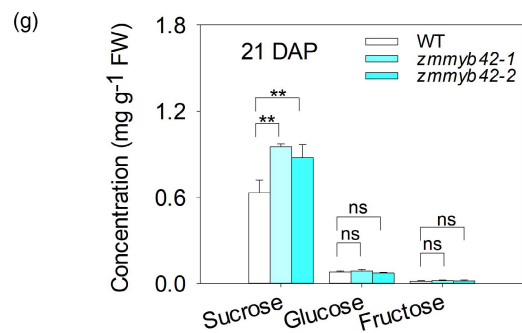
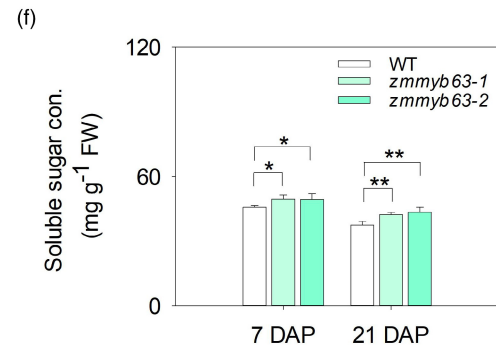
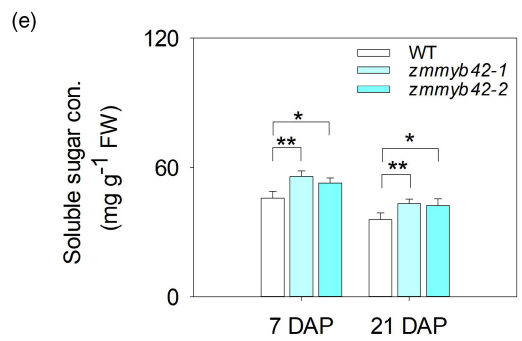
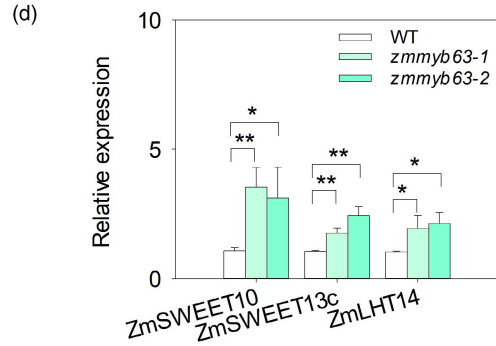
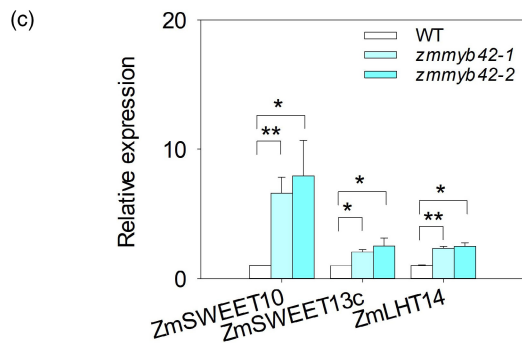
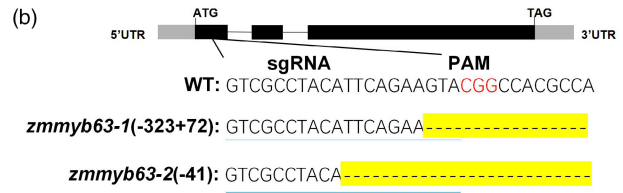


**Figure 4** Accumulation of soluble sugars and free amino acids in *ZmMYB42* and *ZmMYB63* knockout kernels. (a–b) Gene structure of *ZmMYB42* (a) and *ZmMYB63* (b) and mutation sites of the representative mutant lines. The black boxes represent exons, the lines represent introns, and the grey boxes represent the untranslated regions. The sgRNA target sequence is underlined and the PAM motif is highlighted in red. (c–d) Relative expression of *ZmSWEET10*, *ZmSWEET13c* and *ZmLHT14* in *zmyyb42* and *zmyyb63* kernels at 7 DAP in comparison with the wild type. (e–j) Soluble sugar (e–f), individual sugar (g–h), and free amino acid (i–j) concentrations (con.) in kernels of *zmyyb42* and *zmyyb63* lines at 7 or 21 DAP (7 or 21 days after pollination). Error bars represent the SD of three (c–d) or four (e–j) biological replicates. Asterisks indicate significant differences relative to WT as determined by the two-tailed Student's *t*-test (\* $P < 0.05$ ; \*\* $P < 0.01$ ). ns, no significant difference. [Correction added on 4 December 2024, after first online publication: Figure 4's legend has been updated in this version.]

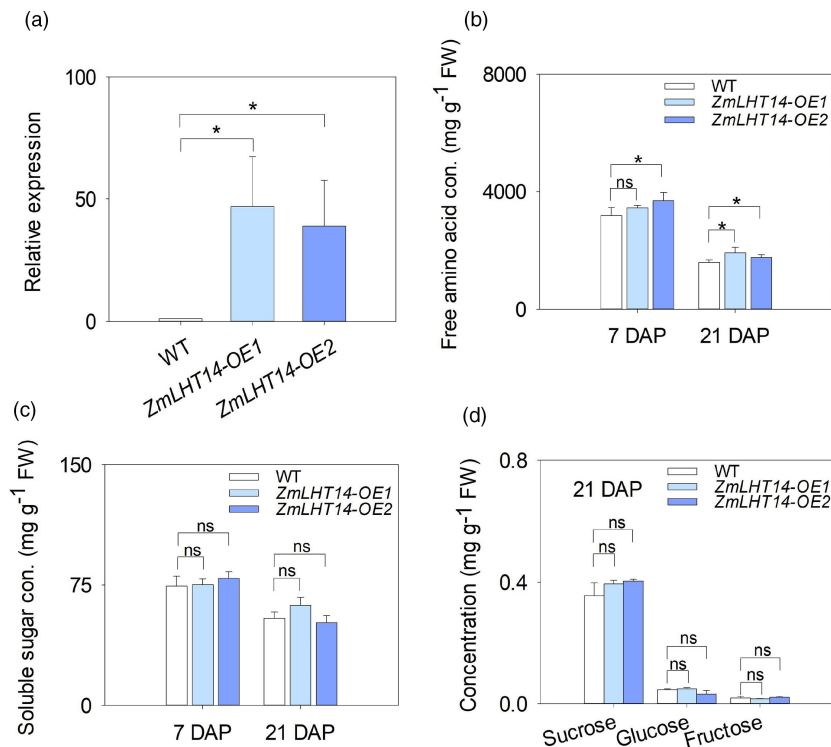


**Figure 5** Accumulation of soluble sugars and free amino acids in *ZmLHT14* overexpression kernels. (a) Relative expression of *ZmLHT14* in kernels of two representative overexpression lines at 7 days after pollination (DAP). (b–d) Free amino acid (b) and soluble sugar (c–d) concentrations (con.) in kernels of *ZmLHT14* overexpression lines at 7 or 21 DAP (7 or 21 days after pollination). Error bars represent the SD of three (a) or four (b–d) biological replicates. Asterisks indicate significant differences relative to WT as determined by the two-tailed Student's *t*-test (\* $P < 0.05$ ; \*\* $P < 0.01$ ). ns, no significant difference.

3 days. Field experiments with four biological replicates were conducted at the Langfang Experimental Station (Heibei). The maize ear and kernels were harvested at 7 or 21 days after pollination (DAP). All samples were immediately frozen in liquid nitrogen and kept in the  $-80^{\circ}\text{C}$  freezer for further analysis.

The inbred line B104 and representative *ZmCCD8* knockout and overexpression lines were used for strigolactone analysis. Seedlings were grown in 50 mL falcon tubes in the greenhouse with 17/7-h light/dark photoperiod, 22/28  $^{\circ}\text{C}$  day/night temperature, and 70% relative humidity for 2 weeks and then under phosphate starvation for 1 week to collect root samples with dramatically enhanced SL production.

#### Reverse transcription-quantitative PCR (RT-qPCR), gene cloning and subcellular localization

The RNA was extracted from the kernel of maize plants using the TRIZOL reagent (Invitrogen, CA, USA) and the cDNA was synthesized using PrimeScript<sup>TM</sup> RT reagent Kit with gDNA Eraser

(Takara, Shiga, Japan) following the manufacturer's instruction. RT-qPCR was conducted to determine gene expression levels by using the TB Green<sup>®</sup> Premix Ex Taq<sup>TM</sup> (Takara, Shiga, Japan). *ZmUbi* was used as the internal control. Each gene had three biological replicates and three technical replicates. The genes specific primers are listed in Table S4.

The full-length coding sequence lacking the termination codon of *ZmUB3*, *ZmMYB42*, *ZmMYB63*, *ZmSWEET10*, *ZmSWEET13* and *ZmLHT14* were cloned into the pSuper1300 vector for GFP-fused protein expression and transformed into *Agrobacterium tumefaciens* strain GV3101. *NF-YA4-mCherry* and *AtCBL1-OPF* constructs were used as a nucleus and plasma membrane marker, respectively, with the empty pSuper1300 vector as a negative control (Batistić *et al.*, 2008; Zhang *et al.*, 2019). The constructs were separately transformed into *Nicotiana benthamiana* leaves, and after 48 h infiltration, fluorescence signals were observed using a Zeiss confocal microscope. The primers are listed in Table S4.

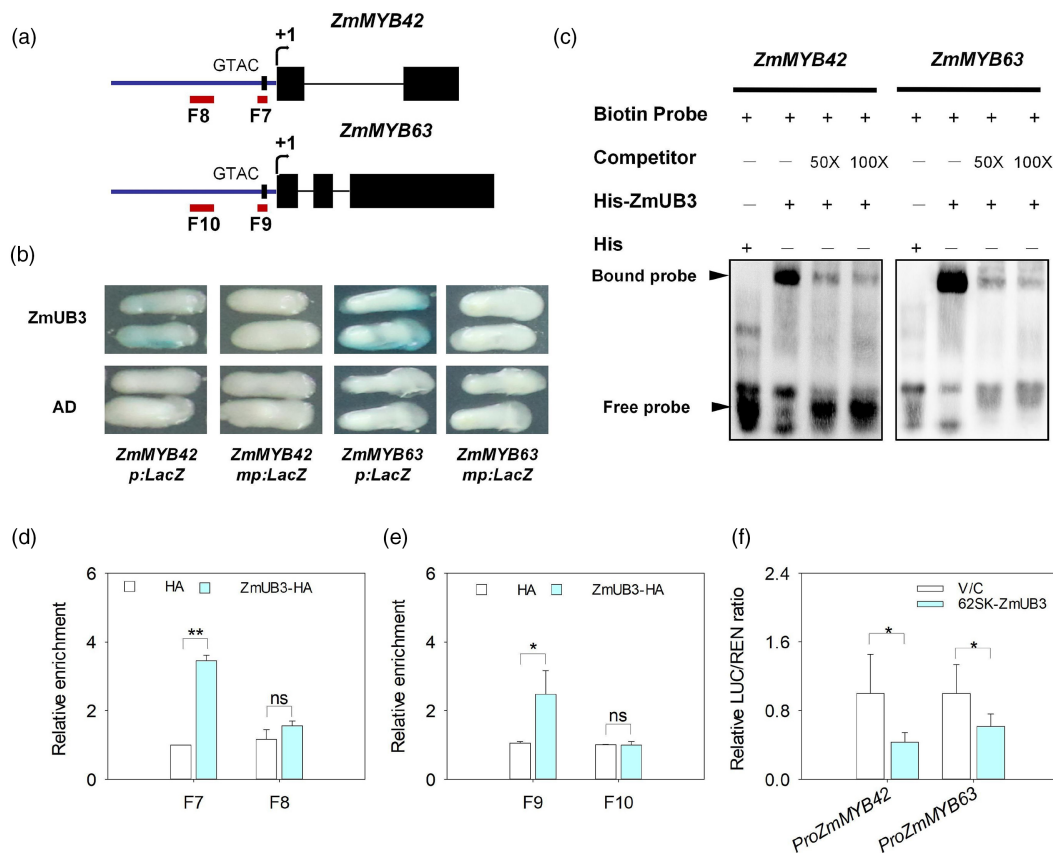


**Figure 6** Regulation of *ZmMYB42* and *ZmMYB63* by ZmUB3s. (a) The GTAC elements in the *ZmMYB42* and *ZmMYB63* promoter. Black boxes represent exons. F7/F9 are GTAC-containing fragments and F8/F10 correspond non-GTAC control fragments. (b) Yeast one-hybrid assay showing that ZmUB3 directly binds to GTAC elements of *ZmMYB42* and *ZmMYB63*. The empty vector AD and GTAC mutants (*mp*) are used as negative control. (c) EMSA showing binding of ZmUB3 to the biotin-labelled GTAC-containing oligonucleotides of *ZmMYB42* and *ZmMYB63* promoters. Black triangles indicate bound and free probes, respectively. (d and e) ChIP-qPCR showing binding of ZmUB3 to the GTAC-containing fragment in the promoter of *ZmMYB42* (d) and *ZmMYB63* (e). (f) Transient expression assay showing down-regulation of *ZmMYB42* and *ZmMYB63* by ZmUB3 (62SK-ZmUB3) compared to the vector control (V/C). Error bars represent the SD of three (d, e) or five (f) biological replicates. Asterisks indicate significant differences relative to the vector control as determined by the two-tailed Student's *t*-test (\* $P < 0.05$ ; \*\* $P < 0.01$ ). ns, no significant difference.

### Constructs and generation of transgenic plants

To generate the construct for CRISPR/Cas9 mediated *ZmCCD8*, *ZmMYB42* and *ZmMYB63* editing, the 20-bp sgRNA (CTATGGCTTCGTCGTTGTGC, CACGCTTGAGGTCAGGGCGA, GTCGCCTACATTCAGAAGTA) was inserted into the pCAMBIA3301 vector, respectively. To obtain *ZmCCD8*, *ZmD14B* and *ZmLHT14* overexpression lines, their full-length coding sequences were amplified and cloned into pCAMBIA3301 to generate *Pro35S:ZmCCD8*, *Pro35S:ZmD14B* and *Pro35S:ZmLHT14* constructs. The recombinant constructs were transformed into the *Agrobacterium tumefaciens* strain EHA105 as previously described (Zhu et al., 2016). The *ZmCCD8* CRISPR/Cas9 and *Pro35S:ZmCCD8* constructs were then transformed into maize embryos of the inbred line B104. The *ZmD14B* and *ZmLHT14* overexpression lines were generated by transforming *Pro35S:ZmD14B* and *Pro35S:ZmLHT14* constructs into maize embryos, and seeds were kindly provided by Center for Crop Functional Genomics and Molecular Breeding of China Agricultural University. At least three independent knockout and/or six overexpression lines for each gene were selected for soil

experiments and two representative lines were then chosen for further characterization. T2 or T3 homozygous transgenic lines were used in this study for phenotype observation and related analysis.

### Strigolactone extraction and quantification

SL extraction and quantification with root tissues were performed following a slightly modified protocol (Charnikhova et al., 2017; Chu et al., 2017; Li et al., 2023). Briefly, maize roots were homogenized to a fine powder in liquid nitrogen and extracted with acetone containing the internal standard GR24. SL was purified using Sep-Pak silica solid-phase extraction cartridges (Waters, Milford, MA, USA), eluted by ethyl acetate, dissolved in 50% acetonitrile in water, and analysed by a UPLC-MS/MS system: the UPLC system (Waters, Milford, MA, USA) equipped with BEH C18 column (1.7  $\mu$ m, 100  $\times$  2.1 mm, Waters, Milford, MA, USA) and a QTRAP 6500 mass spectrometer (AB SCIEX) equipped with an electrospray ionization source. Selected multiple reaction monitoring transitions were 377.1 > 97.1 for zealactone and 299.1 > 97.1 for GR24. The analysis included four biological replicates.

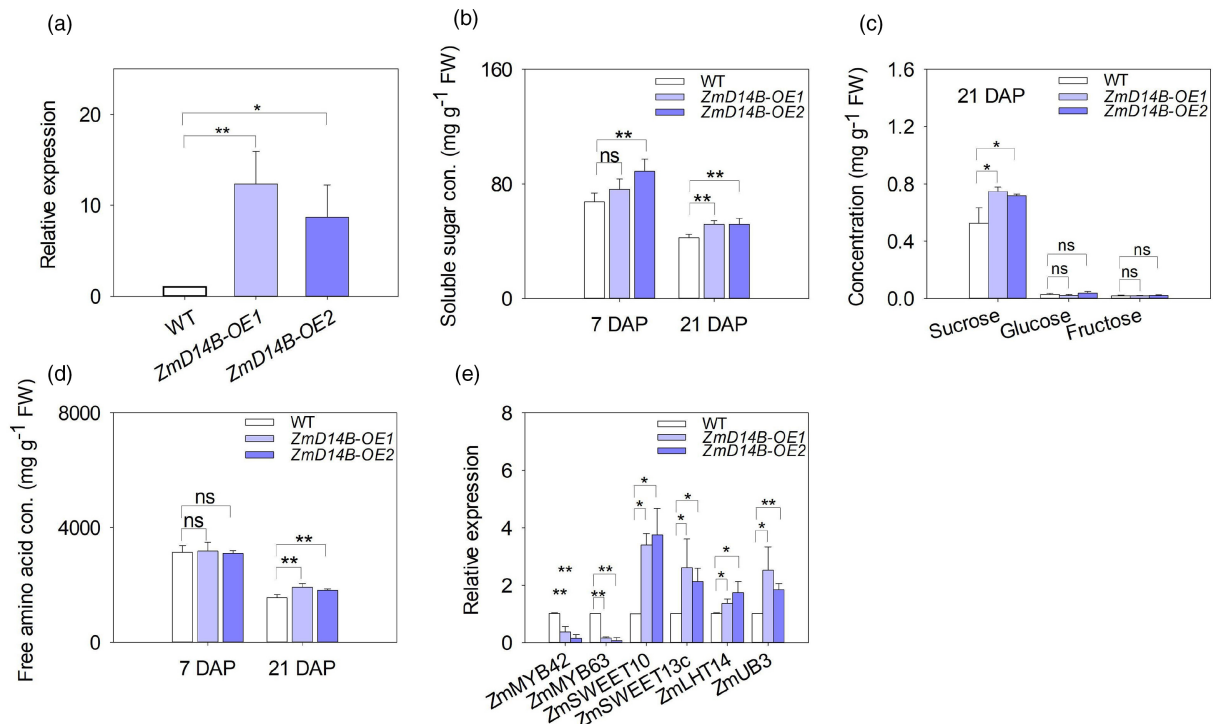


**Figure 7** Accumulation of soluble sugars and free amino acids in *ZmD14B* overexpression kernels. (a) Relative expression of *ZmD14B* in kernels of two representative overexpression lines at 7 days after pollination. (b-d) Soluble sugar (b), individual sugar (c), and free amino acid (d) concentrations (con.) in kernels of *ZmD14B* overexpression lines at 7 or 21 DAP (7 or 21 days after pollination). (e) Relative expression of *ZmMYB42*, *ZmMYB63*, *ZmSWEET10*, *ZmSWEET13c*, *ZmLHT14* and *ZmUB3* in *ZmD14B* overexpression kernels at 7 DAP in comparison to the wild type. Error bars represent the SD of three (a, e) or four (b-d) biological replicates. Asterisks indicate significant differences relative to WT as determined by the two-tailed Student's *t*-test (\* $P < 0.05$ ; \*\* $P < 0.01$ ). ns, no significant difference.

### Soluble sugar and free amino acid measurements

For soluble sugar analysis, 0.1 g of liquid nitrogen-ground tissue was incubated with 1 mL of 80% (v/v) ethanol at 80 °C for 30 min, centrifuged for 5 min at 12000 g at room temperature, and the liquid supernatant was transferred. Repeated this step once and mixed the supernatant. The soluble sugar concentration was determined by the anthrone-sulphuric acid method with glucose as a standard. Measurements of individual sugar were obtained by high-performance liquid chromatography (HPLC). Approximately 1 g of fresh samples were incubated with 5 mL 80% (v/v) ethanol at 80 °C for 30 min and centrifuged at 12000 g for 5 min at room temperature. After filtration, the supernatant was collected for HPLC assay. The Shimadzu HPLC was equipped with a refractive index detector and XN-NH2 column (4.6 × 250 mm; 5 μm; GL Sciences, Tokyo, Japan). The mobile phase was acetonitrile/water (75:25, v/v) with a flow rate of 1 mL min<sup>-1</sup>. Standard sucrose, glucose and fructose were purchased from Dr. Ehrenstorfer (Augsburg, Germany). All solvents were from Thermo Scientific (MA, USA).

Total free amino acids were analysed using the Rosen ninhydrin colorimetric method with Leu as a standard (Rosen, 1957). The amino acid profile was analysed by liquid chromatography–mass spectrometry (LC–MS) following the previous protocol (Hassan *et al.*, 2020). Briefly, fresh kernel samples were freeze-dried and ~20 mg dry samples were sonicated in 1 mL deionized water for 30 min. After centrifugation at 14000 rpm for 10 min

at room temperature, the supernatant was filtered by a 0.11 μm syringe filter. The filtrate was used for derivatization by the AccQ-Tag amino acid analysis kit (Waters, Milford, MA, USA). 80 μL sample was injected into the HPLC column for LC–MS assay according to the manufacturer protocol (Waters, Milford, MA, USA). The amino acid standard was purchased from Waters (Milford, MA, USA).

### RNA isolation, library construction and transcriptome sequencing

Total RNA was extracted from kernels of WT, *ZmCCD8* knockout, and overexpression plants grown in the field 1 week after pollination, followed by library construction and RNA sequencing according to detailed protocols described previously (Pan *et al.*, 2015). After initial screening and trimming, clean reads were mapped to the B73 reference genome (V4) using the Tophat 2.0.6 software (Trapnell *et al.*, 2012). Differentially expressed genes (DEGs) were calculated using Cuffdiff (Trapnell *et al.*, 2012), with the fold change >2 and the false discovery rate <0.05 as a threshold. Two representative transgenic lines (*zmccd8-1*, *ZmCCD8-OE1*) with three biological replicates were selected for sequencing. The Venn diagram was drawn to analyse DGEs between WT and *ZmCCD8* transgenic kernels (<https://bioinformatics.psb.ugent.be/webtools/Venn/>). Pathway enrichment was conducted using the Mapman toolkit with default setting (<https://mapman.gabipd.org/>). The heat map was generated with the R package pheatmap (<https://cran.r-project.org/web/packages/pheatmap/index.html>).

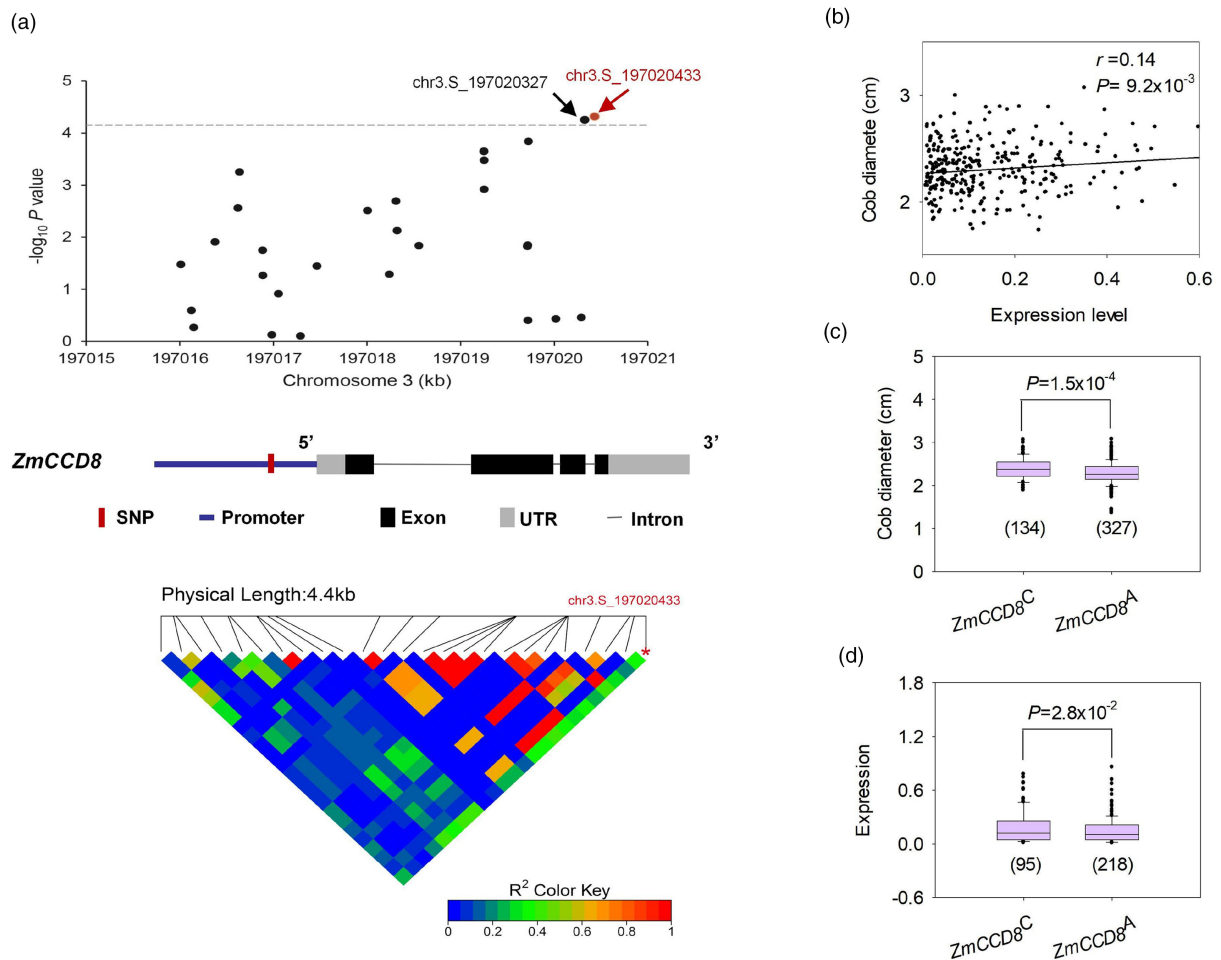


**Figure 8** Natural variations in the promoter of *ZmCCD8* associated with ear traits. (a) GWAS showing association of *ZmCCD8* with the cob diameter. The dot plot includes a partial Manhattan plot, the candidate gene structure and a linkage disequilibrium (LD) heat map. SNP (chr3.S\_197020433) is highlighted in red. (b) Correlation between *ZmCCD8* expression and cob diameter.  $r$ , Pearson correlation coefficient;  $P$ , significance of the linear relationship. (c and d) Boxplots of the cob diameter (c) and expression of *ZmCCD8* (d) in two different haplotypes of the highlighted SNP (chr3.S\_197020433). The  $P$  values in the box plots (c, d) are derived from two-tailed Student's  $t$ -tests.

### Yeast complementation assay

The coding sequences of *ZmSWEET10*, *ZmSWEET13c*, and *sucrose transporter 2* in *Arabidopsis* (*SUC2*, AT1G22710) were cloned into the pDR195 vector and transformed into the sucrose uptake deficient *Saccharomyces cerevisiae* SUSY7/ura3 strain (Wieczorke *et al.*, 1999). The empty pDR195 vector was transformed into the mutant strain SUSY7/ura3 as a native control and *AtSUC2* transformed into the SUSY7/ura3 as a positive control. The positive transformants were selected on agar medium with yeast nitrogen base (YNB) (without uracil) plus ammonium sulphate and 2% glucose. Then, the dilutions ( $1 \times$ ,  $10^{-1} \times$ ,  $10^{-2} \times$ ,  $10^{-3} \times$ ,  $10^{-4} \times$ ) of *ZmSWEET10*, *ZmSWEET13c* and *AtSUC2* yeast cell suspensions were plated on solid synthetic deficient (SD) media including 2% glucose (control) or 2% sucrose. Yeast cell growth was recorded and photographed after incubation at 30 °C for 2 days. The primers are listed in Table S4.

### Yeast one-hybrid assay

Coding sequences of *ZmMYB42*, *ZmMYB63* and *ZmUB3* were inserted into the pB42AD vector (effector). The ~500 bp

promoter fragments of *ZmSWEET10*, *ZmSWEET13c* and *ZmLHT14* containing the MBS (TAACGT or CCGTTG) elements or three tandem repeat elements of *ZmMYB42* and *ZmMYB63* containing the GATC motif were cloned into the placZi2u vector (reporter). The mutated MBS (AAAAAA) and mutant ATAC motif were used as negative controls. The effector and corresponding reporter vectors were co-transformed into the EGY48 yeast strain. Yeast transformation was carried out according to the Yeast Protocols Handbook instructions (Clontech, CA, USA). Transformants were grown on (Trp/-Ura) dropout plates containing 40  $\mu$ g/mL 5-bromo-4-chloro-3-indolyl  $\beta$ -D-galactopyranoside for blue colour development. All primers are listed in Table S4.

### EMSA

The full-length coding sequences of *ZmMYB42*, *ZmMYB63* and *ZmUB3* were separately cloned into the PET-30a vector. The fusion plasmids were transformed into the BL21 strain. The recombinant proteins were purified with Ni-NTA-Agarose. EMSA was then performed following instructions of the Light-Shift® Chemiluminescent EMSA Kit (Thermo Scientific). The ~40 bp probe containing the MBS element of *ZmSWEET10*,



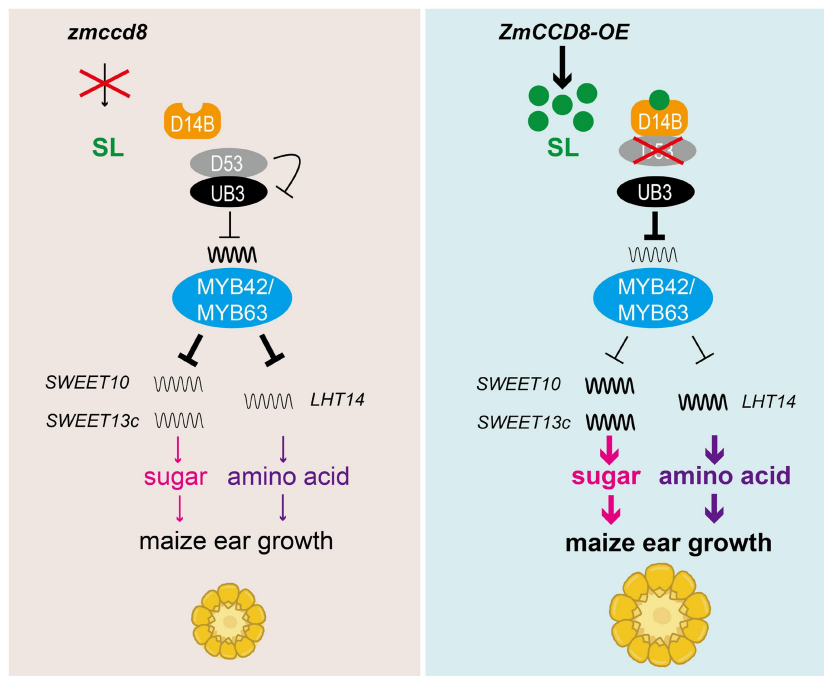


**Figure 9** A schematic model for regulation of sugar and amino acid accumulation by *ZmCCD8* in maize kernels. In *ZmCCD8* knockout (*zmccd8*) lines blocking SL biosynthesis, D53 interacts with UB3 to repress its functioning, ZmMYB42 and ZmMYB63 repress the expression of *ZmSWEET10*, *ZmSWEET13c* and *ZmLHT14* to reduce sugar and amino acid accumulation in kernels and hinder their growth. However, in *ZmCCD8* overexpression (*ZmCCD8-OE*) lines, *ZmCCD8* promotes SL biosynthesis, which is perceived by D14 and triggers degradation of the D53 protein and subsequent UB3 release. UB3 represses the expression of *ZmMYB42* and *ZmMYB63*, allowing up-regulation of *ZmSWEET10*, *ZmSWEET13c* and *ZmLHT14* expression for enhanced accumulation of soluble sugars and free amino acids in kernels and superior growth. Arrow, activation; Bar, repression.

*ZmSWEET13c* and *ZmLHT14* or the GTAC elements of *ZmMYB42* and *ZmMYB63* were synthesized and labelled with biotin, with the biotin unlabelled probe as the negative control. All primers and oligonucleotides are listed in Table S4.

**ChIP assay**

Coding sequences of *ZmMYB42*, *ZmMYB63* and *ZmUB3* were fused to the pUC19-35S-HA-RBS vector and transformed into maize protoplasts of 14-day-old B73 seedlings for overnight culture at 28 °C. The empty pUC19-35S-HA-RBS vector was transformed as a negative control. The ChIP and RT-qPCR assay were performed according to the well-established protocol (Wang *et al.*, 2021). Briefly, the transgenic protoplasts were treated with 1% (v/v) formaldehyde to crosslink protein-DNA complexes and the reaction was terminated by adding 0.125 M glycine. The HA antibodies (Kangwei, Beijing, China) and anti-HA M2 affinity agarose beads (Sigma-Aldrich, MA, USA) were used for ChIP. The immunoprecipitated DNA was purified using QIAquick PCR Purification Kit (QIAGEN, Hilden, Germany). RT-qPCR was performed to analyse enrichment of target fragments with the negative control (the fraction derived from transformation with the empty vector). All primers for ChIP-qPCR are listed in Table S4.

**DLR assay**

Coding sequences of *ZmMYB42*, *ZmMYB63* and *ZmUB3* were inserted into the pGreen 62-SK vector as effectors, and promoters of *ZmSWEET10* (−2 ~ −2019 bp), *ZmSWEET13c* (−3 ~ −1933 bp), *ZmLHT14* (−1 ~ −2077 bp), *ZmMYB42* (−99 ~ −2456 bp) and *ZmMYB63* (−68 ~ −1919 bp) were

cloned into the pGreen II 0800-LUC vector as the reporter. The fusion effector and reporter plasmids were transformed into the *Agrobacterium* GV3101 (pSOUP 19) and co-infiltrated into tobacco leaves. The empty vector was used as the negative control. After 3 days, activities of firefly luciferase (LUC) and Renilla luciferase (REN) were determined using the Dual Luciferase Assay System kit (Promega, WI, USA). The ratio of LUC to REN was calculated with five biological replicates, with the value of the vector control normalized to 1. Primers were listed in Table S4.

**Genome-wide association study (GWAS)**

Genotype and ear-related phenotype data of 508 maize inbred lines were retrieved from the public database MaizeGo (<http://www.maizego.org/>) (Liu *et al.*, 2017; Yang *et al.*, 2014) for genome-wide association study. These inbred lines have tropical, subtropical and temperate origins to represent the global diversity of maize germplasms. Genotyping data with minor allele frequency (MAF) below 0.05 were filtered to implement genome-wide association analysis with a general linear model where the first three principal components were used to control population structure in R package GAPIT (v3) (Wang and Zhang, 2021). A strict significance threshold (−log<sub>10</sub>P = 4.15) was applied according to the previously described method (Ren *et al.*, 2022). Twenty-nine SNPs within 2 kb upstream of the start codon and 2 kb downstream of the stop codon of *ZmCCD8* (GRMZM2G446858) were used to calculate the pairwise linkage disequilibrium in R package Ldheatmap (<https://sfustatgen.github.io/Ldheatmap/>). The position weight matrix was generated by using JASPAR (<https://jaspar.genereg.net/>).

## Statistical analysis

Significance analysis was performed using the two-tailed Student's *t* test for pairwise comparison in SAS (V8, SAS Institute Inc., NC, USA). Means of different treatments were compared based on the least significant difference at a 0.05 or 0.01 level of probability.

## Author contributions

X.L. and Y.Z. designed the study; Y.Z., Y.W., X.P., R.W., D.L., W.R., Z.H., X.S., J.G., E.R., M.S., J.Y., J.C. and Y.X. performed the experiment and collected the data; L.C. performed plasmid construction, genetic transformation, seed propagation and preliminary phenotype observation. Y.Z. and X.L. wrote the paper; P.Y., H.B., W.L., Z.D., Y.W., X.Z., F.Z. and X.L. revised the manuscript.

## Acknowledgements

This work was supported by the National Key Research and Development Program of China (2021YFF1000500), the NSFC grant (31972491), and the China Postdoctoral Science Foundation (2022 M713396). We thank Shuaisong Zhang for kind assistance in plasmid construction and genetic transformation and Prof. Xiaolei Sui (China Agricultural University) for donating the yeast strain SUSY7/ura3 for the sucrose transport activity assay. We also thank Prof. Michael J. Scanlon (Cornell University) and Prof. R. Kelly Dawe (University of Georgia) for editing the manuscript.

## Competing interest statement

The authors declare no competing interests.

## Data availability

All data supporting the findings of this work are included in the manuscript and its Supplementary Information. The phenotyping and genotyping data for the GWAS assay are downloaded from the public database (<http://www.maizego.org/>). The transcriptome data were deposited under the accession code PRJNA978351 in the NCBI Sequence Read Archive (<https://www.ncbi.nlm.nih.gov/>).

## References

- Abe, S., Sado, A., Tanaka, K., Kisugi, T., Asami, K., Ota, S., Kim, H. *et al.* (2014) Carlactone is converted to carlactonoic acid by MAX1 in *Arabidopsis* and its methyl ester can directly interact with AtD14 in vitro. *Proc. Natl. Acad. Sci. U. S. A.* **111**, 18084–18089.
- Akiyama, K., Matsuzaki, K. and Hayashi, H. (2005) Plant sesquiterpenes induce hyphal branching in arbuscular mycorrhizal fungi. *Nature* **435**, 824–827.
- Alder, A., Jamil, M., Marzorati, M., Bruno, M., Vermathen, M., Bigler, P., Ghisla, S. *et al.* (2012) The path from  $\beta$ -carotene to carlactone, a strigolactone-like plant hormone. *Science* **335**, 1348–1351.
- Arite, T., Iwata, H., Ohshima, K., Maekawa, M., Nakajima, M., Kojima, M., Sakakibara, H. *et al.* (2007) DWARF10, an RMS1/MAX4/DAD1 ortholog, controls lateral bud outgrowth in rice. *Plant J.* **51**, 1019–1029.
- Auldridge, M.E., Block, A., Vogel, J.T., Dabney-Smith, C., Mila, I., Bouzayen, M., Magallanes-Lundback, M. *et al.* (2006) Characterization of three members of the *Arabidopsis* carotenoid cleavage dioxygenase family demonstrates the divergent roles of this multifunctional enzyme family. *Plant J.* **45**, 982–993.
- Batistić, O., Sorek, N., Schultke, S., Yalovsky, S. and Kudla, J. (2008) Dual fatty acyl modification determines the localization and plasma membrane targeting of CBL/CIPK Ca<sup>2+</sup> signaling complexes in *Arabidopsis*. *Plant Cell* **20**, 1346–1362.
- Bezruczyk, M., Hartwig, T., Horschman, M., Char, S.N., Yang, J., Yang, B., Frommer, W.B. *et al.* (2018) Impaired phloem loading in *zmsweet13a,b,c* sucrose transporter triple knock-out mutants in *Zea mays*. *New Phytol.* **218**, 594–603.
- Bihmidine, S., Hunter, C.T., Johns, C.E., Koch, K.E. and Braun, D.M. (2013) Regulation of assimilate import into sink organs: update on molecular drivers of sink strength. *Front. Plant Sci.* **4**, 177.
- Braun, D.M., Wang, L. and Ruan, Y.L. (2014) Understanding and manipulating sucrose phloem loading, unloading, metabolism, and signalling to enhance crop yield and food security. *J. Exp. Bot.* **65**, 1713–1735.
- Cantarero, M.G., Cirilo, A.G. and Andrade, F.H. (1999) Night temperature at silking affects set in maize. *Crop. Sci.* **39**, 703–710.
- Charnikhova, T.V., Gaus, K., Lumbroso, A., Sanders, M., Vincken, J.-P., De Mesmaeker, A., Ruyter-Spira, C.P. *et al.* (2017) Zealactones. Novel natural strigolactones from maize. *Phytochemistry* **137**, 123–131.
- Chen, L. and Bush, D. (1997) LHT1, a lysine- and histidine-specific amino acid transporter in *Arabidopsis*. *Plant Physiol.* **115**, 1127–1134.
- Chen, X., Yao, Q., Gao, X., Jiang, C., Harberd, N.P. and Fu, X. (2016) Shoot-to-root mobile transcription factor HY5 coordinates plant carbon and nitrogen acquisition. *Curr. Biol.* **26**, 640–646.
- Chu, J., Fang, S., Xin, P., Guo, Z. and Yi, C. (2017) Quantitative analysis of plant hormones based on LC-MS/MS. In *Hormone Metabolism and Signalling in Plants* (Li, J., Li, C. and Smith, S.M., eds), pp. 471–526. New York, NY: Academic Press.
- Crawford, T., Rendig, V. and Broadbent, F. (1982) Sources, fluxes, and sinks of nitrogen during early reproductive growth of maize (*Zea mays* L.). *Plant Physiol.* **70**, 1654–1660.
- Czarnecki, O., Yang, J., Weston, D., Tuskan, G. and Chen, J.G. (2013) A dual role of strigolactones in phosphate acquisition and utilization in plants. *Int. J. Mol. Sci.* **14**, 7681–7701.
- Gomez-Roldan, V., Fermas, S., Brewer, P.B., Puech-Pagès, V., Dun, E.A., Pillot, J.P., Letisse, F. *et al.* (2008) Strigolactone inhibition of shoot branching. *Nature* **455**, 189–194.
- Guan, J.C., Koch, K.E., Suzuki, M., Wu, S., Latshaw, S., Petrucci, T., Goulet, C. *et al.* (2012) Diverse roles of strigolactone signaling in maize architecture and the uncoupling of a branching-specific subnetwork. *Plant Physiol.* **160**, 1303–1317.
- Guan, J.C., Li, C., Flint-Garcia, S., Suzuki, M., Wu, S., Saunders, J.W., Dong, L. *et al.* (2022) Maize domestication phenotypes reveal strigolactone networks coordinating grain size evolution with kernel-bearing cupule architecture. *Plant Cell* **35**, 1013–1037.
- Guo, N., Gu, M., Hu, J., Qu, H. and Xu, G. (2020a) Rice OsLHT1 functions in leaf-to-panicle nitrogen allocation for grain yield and quality. *Front. Plant Sci.* **11**, 1150.
- Guo, N., Hu, J., Yan, M., Qu, H., Luo, L., Tegeder, M. and Xu, G. (2020b) *Oryza sativa* lysine-histidine-type transporter 1 functions in root uptake and root-to-shoot allocation of amino acids in rice. *Plant J.* **103**, 395–411.
- Ha, C.V., Leyva-Gonzalez, M.A., Osakabe, Y., Tran, U.T., Nishiyama, R., Watanabe, Y., Tanaka, M. *et al.* (2014) Positive regulatory role of strigolactone in plant responses to drought and salt stress. *Proc. Natl. Acad. Sci. U. S. A.* **111**, 851–856.
- Hassan, M.U., Islam, M.M., Wang, R., Guo, J., Luo, H., Chen, F. and Li, X. (2020) Glutamine application promotes nitrogen and biomass accumulation in the shoot of seedlings of the maize hybrid ZD958. *Planta* **251**, 66.
- Hawkins, R.C. and Cooper, P.J.M. (1981) Growth, development and grain yield of maize. *Exp. Agric.* **17**, 203–207.
- Hirel, B., Le Gouis, J., Ney, B. and Gallais, A. (2007) The challenge of improving nitrogen use efficiency in crop plants: towards a more central role for genetic variability and quantitative genetics within integrated approaches. *J. Exp. Bot.* **58**, 2369–2387.
- Hirner, A., Ladwig, F., Stransky, H., Okumoto, S., Keinath, M., Harms, A., Frommer, W.B. *et al.* (2006) *Arabidopsis* LHT1 is a high-affinity transporter for cellular amino acid uptake in both root epidermis and leaf mesophyll. *Plant Cell* **18**, 1931–1946.

- Jiang, L., Liu, X., Xiong, G., Liu, H., Chen, F., Wang, L., Meng, X. *et al.* (2013) DWARF 53 acts as a repressor of strigolactone signalling in rice. *Nature* **504**, 401–405.
- Kapulnik, Y. and Koltai, H. (2014) Strigolactone involvement in root development, response to abiotic stress, and interactions with the biotic soil environment. *Plant Physiol.* **166**, 560–569.
- Kohlen, W., Charnikhova, T., Lammers, M., Pollina, T., Tóth, P., Haider, I., Pozo, M.J. *et al.* (2012) The tomato *CAROTENOID CLEAVAGE DIOXYGENASE8* (*SICCD8*) regulates rhizosphere signaling, plant architecture and affects reproductive development through strigolactone biosynthesis. *New Phytol.* **196**, 535–547.
- Kong, D., Li, C., Xue, W., Wei, H., Ding, H., Hu, G., Zhang, X. *et al.* (2023) UB2/UB3/TSH4-anchored transcriptional networks regulate early maize inflorescence development in response to simulated shade. *Plant Cell* **35**, 717–737.
- Lalonde, S., Wipf, D. and Frommer, W.B. (2004) Transport mechanisms for organic forms of carbon and nitrogen between source and sink. *Annu. Rev. Plant Biol.* **55**, 341–372.
- Li, S., Tian, Y., Wu, K., Ye, Y., Yu, J., Zhang, J., Liu, Q. *et al.* (2018) Modulating plant growth-metabolism coordination for sustainable agriculture. *Nature* **560**, 595–600.
- Li, C., Dong, L., Durairaj, J., Guan, J.C., Yoshimura, M., Quinodoz, P., Horber, R. *et al.* (2023) Maize resistance to witchweed through changes in strigolactone biosynthesis. *Science* **379**, 94–99.
- Lin, H., Wang, R., Qian, Q., Yan, M., Meng, X., Fu, Z., Yan, C. *et al.* (2009) DWARF27, an iron-containing protein required for the biosynthesis of strigolactones, regulates rice tiller bud outgrowth. *Plant Cell* **21**, 1512–1525.
- Liu, H., Luo, X., Niu, L., Xiao, Y., Chen, L., Liu, J., Wang, X. *et al.* (2017) Distant eQTLs and non-coding sequences play critical roles in regulating gene expression and quantitative trait variation in maize. *Mol. Plant* **10**, 414–426.
- Liu, Y., Wu, G., Zhao, Y., Wang, H.H., Dai, Z., Xue, W., Yang, J. *et al.* (2021) DWARF53 interacts with transcription factors UB2/UB3/TSH4 to regulate maize tillering and tassel branching. *Plant Physiol.* **187**, 947–962.
- Luo, G., Shen, L., Song, Y., Yu, K., Ji, J., Zhang, C., Yang, W. *et al.* (2021) The MYB family transcription factor *TuODORANT1* from *Triticum urartu* and the homolog *TaODORANT1* from *Triticum aestivum* inhibit seed storage protein synthesis in wheat. *Plant Biotechnol. J.* **19**, 1863–1877.
- Martin, A., Lee, J., Kichey, T., Gerentes, D., Zivy, M., Tatout, C., Dubois, F. *et al.* (2006) Two cytosolic glutamine synthetase isoforms of maize are specifically involved in the control of grain production. *Plant Cell* **18**, 3252–3274.
- Pan, X., Hasan, M.M., Li, Y., Liao, C., Zheng, H., Liu, R. and Li, X. (2015) Asymmetric transcriptomic signatures between the cob and florets in the maize ear under optimal- and low-nitrogen conditions at silking, and functional characterization of amino acid transporters *ZmAAP4* and *ZmVAAT3*. *J. Exp. Bot.* **66**, 6149–6166.
- Perchlik, M. and Tegeder, M. (2018) Leaf amino acid supply affects photosynthetic and plant nitrogen use efficiency under nitrogen stress. *Plant Physiol.* **178**, 174–188.
- Ren, W., Zhao, L., Liang, J., Wang, L., Chen, L., Li, P., Liu, Z. *et al.* (2022) Genome-wide dissection of changes in maize root system architecture during modern breeding. *Nat. Plants* **8**, 1408–1422.
- Rosen, H. (1957) A modified ninhydrin colorimetric analysis for amino acids. *Arch. Biochem. Biophys.* **67**, 10–15.
- Sasse, J., Simon, S., Gübeli, C., Liu, G.-W., Cheng, X., Friml, J., Bouwmeester, H. *et al.* (2015) Asymmetric localizations of the ABC transporter PaPDR1 trace paths of directional strigolactone transport. *Curr. Biol.* **25**, 647–655.
- Schobert, C. and Komor, E. (1990) Transfer of amino acids and nitrate from the roots into the xylem of *Ricinus communis* seedlings. *Planta* **181**, 85–90.
- Schussler, J.R. and Westgate, M.E. (1991) Maize kernel set at low water potential: II. sensitivity to reduced assimilates at pollination. *Crop. Sci.* **31**, 1196–1203.
- Seebauer, J.R., Moose, S.P., Fabbri, B.J., Crossland, L.D. and Below, F.E. (2004) Amino acid metabolism in maize earshoots. Implications for assimilate preconditioning and nitrogen signaling. *Plant Physiol.* **136**, 4326–4334.
- Shen, S., Ma, S., Chen, X.M., Yi, F., Li, B.B., Liang, X.G., Liao, S.J. *et al.* (2022) A transcriptional landscape underlying sugar import for grain set in maize. *Plant J.* **110**, 228–242.
- Snowden, K.C., Simkin, A.J., Janssen, B.J., Templeton, K.R., Loucas, H.M., Simons, J.L., Karunairetnam, S. *et al.* (2005) The *Decreased apical dominance1/Petunia hybrida CAROTENOID CLEAVAGE DIOXYGENASE8* gene affects branch production and plays a role in leaf senescence, root growth, and flower development. *Plant Cell* **17**, 746–759.
- Song, X., Lu, Z., Yu, H., Shao, G., Xiong, J., Meng, X., Jing, Y. *et al.* (2017) IPA1 functions as a downstream transcription factor repressed by D53 in strigolactone signaling in rice. *Cell Res.* **27**, 1128–1141.
- Sosso, D., Luo, D., Li, Q.B., Sasse, J., Yang, J., Gendrot, G., Suzuki, M. *et al.* (2015) Seed filling in domesticated maize and rice depends on SWEET-mediated hexose transport. *Nat. Genet.* **47**, 1489–1493.
- Srivastava, A.C., Ganesan, S., Ismail, I.O. and Ayre, B.G. (2008) Functional characterization of the *Arabidopsis* AtSUC2 sucrose/H<sup>+</sup> symporter by tissue-specific complementation reveals an essential role in phloem loading but not in long-distance transport. *Plant Physiol.* **148**, 200–211.
- Sun, H., Guo, X., Zhu, X., Gu, P., Zhang, W., Tao, W., Wang, D. *et al.* (2023) Strigolactone and gibberellin signaling coordinately regulate metabolic adaptations to changes in nitrogen availability in rice. *Mol. Plant* **16**, 588–598.
- Tegeder, M. and Rentsch, D. (2010) Uptake and partitioning of amino acids and peptides. *Mol. Plant* **3**, 997–1011.
- Tollenaar, M., Dwyer, L.M. and Stewart, D.W. (1992) Ear and kernel formation in maize hybrids representing three decades of grain yield improvement in Ontario. *Crop. Sci.* **32**, 432–438.
- Trapnell, C., Roberts, A., Goff, L., Pertea, G., Kim, D., Kelley, D.R., Pimentel, H. *et al.* (2012) Differential gene and transcript expression analysis of RNA-seq experiments with TopHat and Cufflinks. *Nat. Protoc.* **7**, 562–578.
- Ueda, H. and Kusaba, M. (2015) Strigolactone regulates leaf senescence in concert with ethylene in *Arabidopsis*. *Plant Physiol.* **169**, 138–147.
- Umehara, M., Hanada, A., Yoshida, S., Akiyama, K., Arite, T., Takeda-Kamiya, N., Magome, H. *et al.* (2008) Inhibition of shoot branching by new terpenoid plant hormones. *Nature* **455**, 195–200.
- Wang, J. and Zhang, Z. (2021) GAPIT Version 3: boosting power and accuracy for genomic association and prediction. *Genomics Proteomics Bioinformatics* **19**, 629–640.
- Wang, L., Wang, B., Yu, H., Guo, H., Lin, T., Kou, L., Wang, A. *et al.* (2020) Transcriptional regulation of strigolactone signalling in *Arabidopsis*. *Nature* **583**, 277–281.
- Wang, R., Zhong, Y., Liu, X., Zhao, C., Zhao, J., Li, M., Ul Hassan, M. *et al.* (2021) Cis-regulation of the amino acid transporter genes *ZmAAP2* and *ZmLHT1* by *ZmPHR1* transcription factors in maize ear under phosphate limitation. *J. Exp. Bot.* **72**, 3846–3863.
- Wei, L., Mao, W., Jia, M., Xing, S., Ali, U., Zhao, Y., Chen, Y. *et al.* (2018) FaMYB44.2, a transcriptional repressor, negatively regulates sucrose accumulation in strawberry receptacles through interplay with FaMYB10. *J. Exp. Bot.* **69**, 4805–4820.
- Wieczorko, R., Krampe, S., Weierstall, T., Freidel, K., Hollenberg, C.P. and Boles, E. (1999) Concurrent knock-out of at least 20 transporter genes is required to block uptake of hexoses in *Saccharomyces cerevisiae*. *FEBS Lett.* **464**, 123–128.
- Xiao, Q., Wang, Y., Du, J., Li, H., Wei, B., Wang, Y., Li, Y. *et al.* (2017) ZmMYB14 is an important transcription factor involved in the regulation of the activity of the *ZmBT1* promoter in starch biosynthesis in maize. *FEBS J.* **284**, 3079–3099.
- Xuan, Y.H., Hu, Y.B., Chen, L.Q., Sosso, D., Ducat, D.C., Hou, B.H. and Frommer, W.B. (2013) Functional role of oligomerization for bacterial and plant SWEET sugar transporter family. *Proc. Natl. Acad. Sci. U. S. A.* **110**, E3685–E3694.
- Yamada, Y., Otake, M., Furukawa, T., Shindo, M., Shimomura, K., Yamaguchi, S. and Umehara, M. (2018) Effects of strigolactones on grain yield and seed development in rice. *J. Plant Growth Regul.* **38**, 753–764.
- Yang, N., Lu, Y., Yang, X., Huang, J., Zhou, Y., Ali, F., Wen, W. *et al.* (2014) Genome wide association studies using a new nonparametric model reveal the genetic architecture of 17 agronomic traits in an enlarged maize association panel. *PLoS Genet.* **10**, e1004573.
- Yang, B., Wang, J., Yu, M., Zhang, M., Zhong, Y., Wang, T., Liu, P. *et al.* (2022) The sugar transporter *ZmSUGCAR1* of the nitrate transporter 1/peptide transporter family is critical for maize grain filling. *Plant Cell* **34**, 4232–4254.

- Yoneyama, K., Mori, N., Sato, T., Yoda, A., Xie, X., Okamoto, M., Iwanaga, M. et al. (2018) Conversion of carlactone to carlactonoic acid is a conserved function of MAX1 homologs in strigolactone biosynthesis. *New Phytol.* **218**, 1522–1533.
- Zhang, Y., van Dijk, A.D., Scaffidi, A., Flematti, G.R., Hofmann, M., Charnikhova, T., Verstappen, F. et al. (2014) Rice cytochrome P450 MAX1 homologs catalyze distinct steps in strigolactone biosynthesis. *Nat. Chem. Biol.* **10**, 1028–1033.
- Zhang, S., Feng, M., Chen, W., Zhou, X., Lu, J., Wang, Y., Li, Y. et al. (2019) In rose, transcription factor PTM balances growth and drought survival via PIP2;1 aquaporin. *Nat. Plants* **5**, 290–299.
- Zhong, Y., Pan, X., Wang, R., Xu, J., Guo, J., Yang, T., Zhao, J. et al. (2020) *ZmCCD10a* encodes a distinct type of carotenoid cleavage dioxygenase and enhances plant tolerance to low phosphate. *Plant Physiol.* **184**, 374–392.
- Zhou, F., Lin, Q., Zhu, L., Ren, Y., Zhou, K., Shabek, N., Wu, F. et al. (2013) D14-SCF(D3)-dependent degradation of D53 regulates strigolactone signalling. *Nature* **504**, 406–410.
- Zhu, J., Song, N., Sun, S., Yang, W., Zhao, H., Song, W. and Lai, J. (2016) Efficiency and inheritance of targeted mutagenesis in maize using CRISPR-Cas9. *J. Genet. Genomics* **43**, 25–36.
- Zhu, X., Shao, X., Pei, Y., Guo, X., Li, J., Song, X. and Zhao, M. (2018) Genetic diversity and genome-wide association study of major ear quantitative traits using high-density SNPs in maize. *Front. Plant Sci.* **9**, 966.
- Zou, J., Zhang, S., Zhang, W., Li, G., Chen, Z., Zhai, W., Zhao, X. et al. (2006) The rice *HIGH-TILLERING DWARF1* encoding an ortholog of *Arabidopsis* MAX3 is required for negative regulation of the outgrowth of axillary buds. *Plant J.* **48**, 687–698.

## Supporting information

Additional supporting information may be found online in the Supporting Information section at the end of the article.

**Figure S1.** *ZmCCD8* expression in the maize ear.

**Figure S2.** The phenotype of stable transgenic plants of *ZmCCD8* at 21 days after pollination (21 DAP).

**Figure S3.** RT-qPCR analysis with kernel samples of *ZmCCD8* transgenic plants at 7 days after pollination (7 DAP).

**Figure S4.** Subcellular localization of ZmSWEETs, ZmLHT14, ZmMYBs and ZmUB3.

**Figure S5.** The SNP position in the *ZmCCD8* promoter.

**Figure S6.** GWAS showing *ZmCCD8* variations associated with ears traits.

**Table S1.** Significant gene differential expression in *ZmCCD8* knockout (*zmccd8-1*) and WT kernels at 7 DAP.

**Table S2.** Significant gene differential expression in *ZmCCD8* overexpression (*ZmCCD8-OE1*) and WT kernels at 7 DAP.

**Table S3.** The *P* value of 2379 single-nucleotide polymorphisms (SNPs).

**Table S4.** Primers used for gene cloning, expression and vector construction.